Building and Environment 225 (2022) 109616

Contents lists available at ScienceDirect

Building and Environment

journal homepage: www.elsevier.com/locate/buildenv

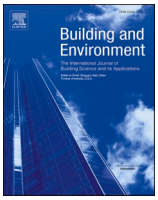

Numerical and experimental study of the dynamic thermal resistance of ventilated air-spaces behind passive and active façades

Mohammad Rahiminejad *, Dolaana Khovalyg

Laboratory of Integrated Comfort Engineering (ICE), Ecole Polytechnique Fédérale de Lausanne (EPFL), Lausanne, Switzerland

ARTICLE INFO

Keywords:
Thermal resistance
Ventilated air-space
Numerical simulations
Experimental measurements
Traditional and BIPV façades

ABSTRACT

The variation of the thermo-hydrodynamic behavior of the airflow in the ventilated cavity behind external claddings in a wall structure could potentially affect the overall thermal resistance of the entire structure. Although the impact of an enclosed air-space in the wall on the total R-value of the assembly has been thoroughly investigated in the literature, it has not been addressed for a ventilated cavity. In the present study, as a first step, plausible definitions to determine the thermal resistance of the ventilated cavity behind external claddings in transient conditions are described. As the second step, the dynamic thermal resistance of the naturally ventilated air-spaces behind passive (i.e., brick and fiber cement) claddings and active (i.e., BIPV) facades are studied using two approaches. In the first approach, a 2-D numerical model validated against measurements is employed to compute the thermal resistance of the ventilated air gap under different conditions. Accordingly, the impact of the cladding type, seasonal variation, cavity thickness, and presence of the reflective insulation in the air gap on the dynamic change of the thermal resistance of the air-space is analyzed. In the second approach, in-field measurements are performed in a test facility to experimentally examine the contribution of the thermal resistance of the cavity to the total R-value of the wall structure. The results obtained from both approaches are compared with the design values calculated based on the ISO 6946:2017 and ISO 9869–1:2014 standards. The results reveal that the dynamic change of the thermal resistance of the air gap during a day could be captured using numerical simulations. It is shown that the daily averaged thermal resistance of the cavity could reach up to 47 times higher than the design R-value of the BIPV façade. The experimental measurements confirm that the thermal resistance of the ventilated air-space could converge to a steady-state value after a certain duration of time following the requirements provided in the standards, which could be practically used for the code-compliant analysis. It is also observed that the ventilated cavity could act as an insulation layer with higher thermal resistance compared to some of the solid materials used in the wall assembly.

1. Introduction

The primary purpose of using ventilated air-spaces behind traditional claddings in the wall structures is to reduce the moisture contents of the wall materials [1,2]. In addition to that, ventilation in the air gap could enhance the thermal performance of the assembly by reducing heat flow losses/gains through the walls [3–6]. The ventilated cavity design parameters could highly affect the energy flows across the wall assembly. The results of the experimental study by Ref. [7] showed that a higher cavity thickness behind a fiber cement cladding could reduce the heat gain through the wall [8]. showed that a higher emissivity of the cavity surface adjacent to the massive wall with a fiber cement cladding could result in a higher heat gain during summer and heat loss during winter. The comparative measurements between a ventilated façade and a conventional single-layer facade conducted by Ref. [9] revealed that up to 11.4% energy saving could be achieved by incorporating a ventilated air-space behind the wooden cladding. The presence of the ventilated cavity in the wall structure could also reduce the point thermal transmittance by decreasing the heat flow through the point thermal bridges [10]. Similar to the traditional (passive) façades, the presence of sub-frames in the Building Integrated Photovoltaic (BIPV) façades creates a ventilated air gap behind the PV modules. In this cladding system, where the traditional external cladding is replaced by PV modules and consequently, could be regarded as an active façade due to the on-site electricity generation, the presence of the ventilated air-space could be even more beneficial compared to the passive claddings. In particular, the BIPV façade as a highly efficient multi-energy

* Corresponding author. EPFL– Fribourg, Passage du Cardinal 13b, CH-1700, Fribourg, Switzerland.
E-mail address: mohammad.rahiminejad@epfl.ch (M. Rahiminejad).

https://doi.org/10.1016/j.buildenv.2022.109616
Received 1 July 2022; Received in revised form 16 August 2022; Accepted 15 September 2022
Available online 21 September 2022

Nomenclature

c_p	Specific heat capacity [J/kg•K]
d	Thickness of the material [m]
Gr	Grashof number [−]
h	Heat transfer coefficient [W/m^2•K]
k	Thermal conductivity [W/m•K]
q	Heat flux [W/m^2]
R	Thermal resistance [W/m^2•K]
Ra	Rayleigh number [−]
Re	Reynolds number [−]
T	Temperature [K]
u	Uncertainty [m^2•K/W or W/m^2•K]
U	Thermal transmittance [m^2•K/W]
α	Absoprtivity [−]
σ	Stefan-Boltzmann constant [W/m^{2}K^4]
ε	Surface emissivity [−]
ρ	Density [kg/m^3]
τ	Transmittance [−]

Subscripts

app	Apparent
ave	Average
cav	Cavity
cl	Cladding
cond	Conduction
conv	Convection
des	Design
eb	Earth brick
exp	Experiment
ext	Exterior
fp	Fiber plaster
ind	Indoor
ins	Insulation
int	Interior
jc	Jute coating
meas	Measured
nat	Natural
out	Outdoor
rad	Radiation
sim	Simulation
sur	Surface
tot	Total
wall	Wall
wc	Wall core
wood	Wood

generation cladding system could yield benefits for ventilation and the thermal performance of the entire assembly. For instance, the dissipated heat from the back of the module could be removed by the airflow through the cavity to reduce its surface temperature and consequently, increase the electrical efficiency of the PV panels [11]. Therefore, the ventilated air gap behind BIPV façades can simultaneously affect the electrical efficiency of PV modules and the thermal efficiency of the entire wall structure [12].

Generally, heat flow reduction through a wall assembly in a building envelope can be achieved using elements with a high thermal resistance (R-value). The R-value of a solid component is a function of the rate of steady-state or time-averaged temperature difference across the element and heat transfer through the structure [13]. Consequently, the R-value of the wall assembly depends on the thermo-physical properties of the materials used in the building and outdoor/indoor thermal conditions. For building energy-saving purposes, the thermal transmittance (U-value), and consequently the R-value, of walls is typically limited by building energy performance standards at the national level (e.g., SIA 380 in Switzerland). In the case of the presence of the ventilated air-space in the wall assembly, the variable thermo-hydrodynamic behavior of the airflow in the cavity is caused by the contribution of several parameters [14], which could strongly affect the total thermal resistance of the entire structure. However, this aspect has not been adequately addressed in the literature. Considering the international norms and standards in which the calculation/measuring methods for the thermal resistance of ventilated walls are described, one can see the scarcity of information and test methods to quantify the thermal resistance caused by the ventilated air cavity. For instance, as stated in the ASHRAE Handbook of Fundamentals [46], all the available procedures to obtain the thermal resistance of a cavity in a wall assembly only applies for ideal conditions, i.e., air-spaces of uniform thickness bounded by plane, smooth, parallel surfaces with no air-leakage to or from the space. In another standard, ISO 6946:2017, a steady-state calculation method is proposed to determine the total thermal resistance of a wall structure, including a ventilated cavity; in the case of a well-ventilated air layer, the method suggests only considering an external surface resistance corresponding to still air and disregard the thermal resistance of the air layer and all other layers between the air layer and external environment. However, the research basis is not reported and does not include any information on how the thermal resistance of the ventilated cavity should be separately obtained.

By reviewing the scientific publications, only a few studies can be found investigating the impact of different parameters on the total R-value of wall structures having a ventilated air-space behind traditional external claddings, although the thermal resistance of wall assemblies with non-ventilated air-spaces has been thoroughly investigated in the literature [15–18]. The results of the research performed by Ref. [19] showed that the overall thermal resistance of the ventilated wall structure could be enhanced by using external claddings with low conductivity. In a test report provided by EXOVA [20], the hot box test method was used to evaluate the thermal resistance of a ventilated wall with vinyl siding. The results indicated that the overall R-value of the entire wall structure increases if the emissivity of the cavity surface is decreased. In an experimental study by Ref. [21]; measurements in general accordance with the standardized hot box method (ASTM 1363–19 [47]) in steady-state conditions are performed to obtain the overall thermal resistance of a ventilated wall structure with brick cladding. The results showed that the total R-value is increased when the airflow is present in the cavity. The experimental results of [3] showed that the total thermal resistance of a prefabricated ventilated wall structure is higher than the design value determined based on [13]; and could be only evaluated reliably under winter conditions. The results of laboratory measurements performed by Ref. [22] showed that the overall thermal resistances of ventilated wall structures with fiber cement and wooden claddings obtained following the criteria specified by Ref. [23] are in good agreement with the calculations based on [13]. The results of an in-field experimental measurement carried out by Ref. [24] revealed that the total thermal resistance of a wall structure with a ventilated cavity was increased by around 78% compared to the wall assembly without a cavity.

The aforementioned literature review highlights the fact that only the overall thermal resistance of the wall structures incorporating ventilated cavities is rarely studied in the previous works, and the thermal resistance of the ventilated air gaps has not been specifically defined. The lack of studies related to the ventilated BIPV systems is even greater, and to the best of the authors' knowledge, the thermal

resistance of the ventilated cavity behind vertical BIPV panels has not been particularly investigated in the literature. To address these limitations, a research project ASHRAE 1759-RP [45] was performed by the authors to provide a theoretical analysis of the thermal resistance of ventilated air-spaces behind vertical claddings. The further objective of this project was to suggest modifications for the standard hot box method to experimentally quantify the thermal resistance of the ventilated cavity in a wall assembly. In the first part, three plausible definitions for the thermal resistance of the ventilated cavity in the steady-state condition were proposed, and the most practical formulation that can be applied in real operating conditions was selected [25]. In the second part, theoretical uncertainty analysis was performed based on the parameters involved in defining the thermal resistance of the ventilated cavity. Accordingly, suggestions on the design of a plausible test setup to incorporate and study airflow effects in a suitable test method were provided [26].

Despite the novelty and originality of the research performed within the framework of the ASHRAE 1759-RP project [45], all of the analysis was provided in the steady-state condition, and the dynamic variation of the thermal resistance of the ventilated air-spaces under transient conditions was not addressed. Moreover, the literature review indicates that the effects of the influential parameters, such as the thickness of the air-space and the emissivity of the cavity surfaces, have not been considered in the previous studies. Furthermore, as mentioned earlier, the thermal resistance of the ventilated air-spaces behind BIPV façades has not been investigated in the previous works. Therefore, the purpose of the present paper is to explore the variation of the thermal resistance of ventilated wall structures with both traditional and BIPV façades in transient conditions under the impact of the dynamic change of the indoor/outdoor weather data. The problem is addressed using two approaches; i.e., experimental measurements and numerical analysis. The former approach is used in a test facility to measure the total R-value of the ventilated wall structure and also to quantify the thermal resistance of the air-space behind its traditional cladding. In the latter approach, a transient numerical model is employed to analyze the contribution of the thermal resistance caused by the air cavity to the total R-value of the building wall assemblies with the passive (traditional) and active (BIPV) claddings. Moreover, using the numerical model, the impacts of the seasonal variation, the thickness of the ventilated air gap, and emissivity of the cavity surface adjacent to the wall core on the thermal resistance of the air-space are evaluated. In the following sections, first, the methodology used to conduct this research is explained in section 2. Thereafter, the results of the numerical simulations and experimental measurements are presented in section 3. In section 4, the discussion of the results is provided by exploring the contribution of the thermal resistance of the ventilated cavities to the total R-value of the wall structures. Conclusive remarks on the present work and suggestions for future studies are presented in section 5.

2. Methodology

In this section, the methodology used to perform analysis on the

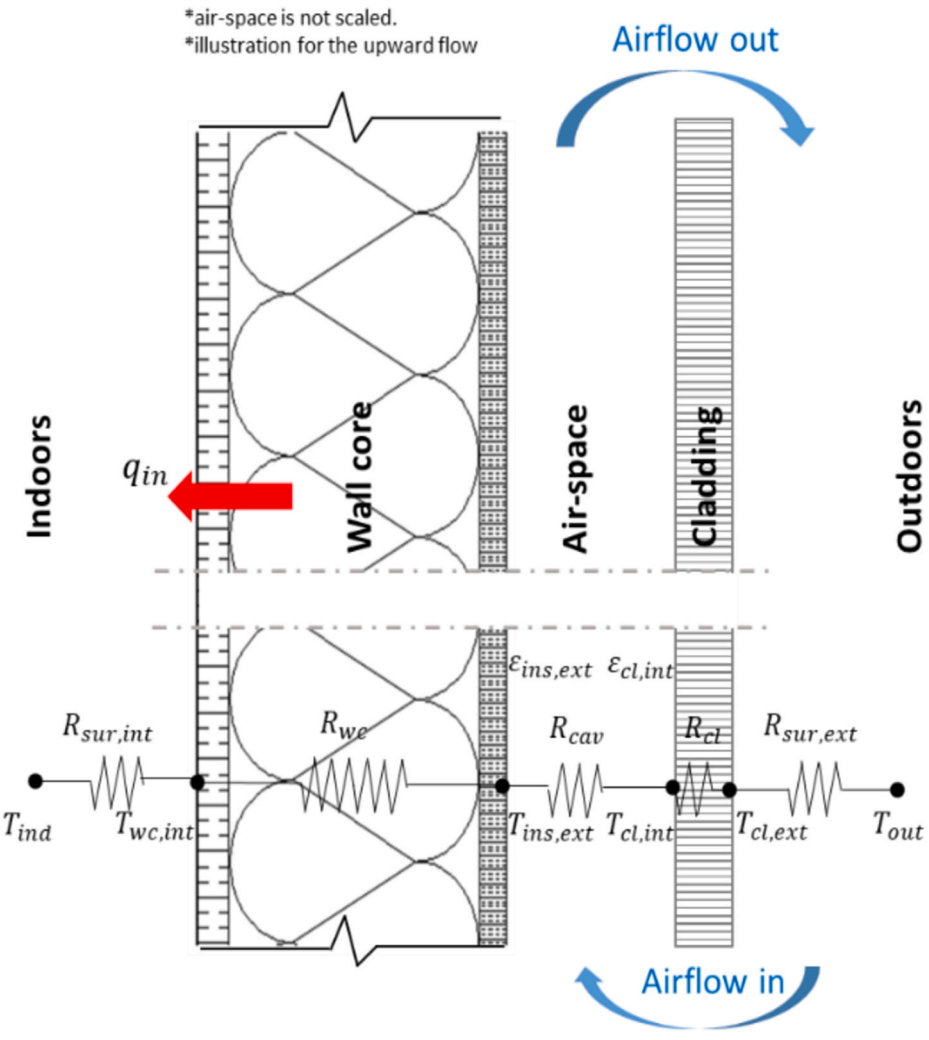

Fig. 1. Schematic representation of a typical ventilated wall structure (adopted from Ref. [25].

thermal resistance of a wall assembly incorporating ventilated cavity is presented. In the following subsections, first, the methods to determine the U-value and R-value of a ventilated wall structure are described following the procedure recommended in the [13,23] standards. Thereafter, different methods that could be numerically or experimentally employed to obtain the thermal resistance of a ventilated air-space in transient conditions are summarized. At the end of this section, the details of the numerical simulations and experimental measurements are elaborated.

2.1. Determination of U-value and R-value of the ventilated walls

An illustration of a typical ventilated wall structure is depicted in Fig. 1. The network of thermal resistances from outdoors to indoors, including surface thermal resistances R_{sur}, R-value of the cladding R_{cl}, thermal resistance of the cavity R_{cav}, and R-value of the wall core R_{wc} are also presented in the illustration. In the present study, the theoretical calculations for the U-value and R-value of the ventilated wall assembly are performed using the recommendations specified in Ref. [13]. The data of the in-field measurements are processed following the procedure explained in Ref. [23]. In the following sections, a summary of the procedure described in the standards is provided.

- Design calculations [13].

According to the description provided in Ref. [13]; the total design thermal resistance $R_{tot,des}$ of the wall structure consisting of uniform layers that are perpendicular to the heat flux shall be calculated based on the inverse of its thermal transmittance according to equation (1) [27–29]:

$$R_{tot,des} = \frac{1}{U} = R_{sur,int} + \sum R_i + R_{sur,ext} \tag{1}$$

where $\sum R_i$ is the summation of the design thermal resistances of the layers used in the wall assembly and $R_{sur,int}$ and $R_{sur,ext}$ are the interior and exterior surface resistances, respectively equal to 0.13 (m^2•K/W) and 0.04 (m^2•K/W); which refer to a horizontal heat flux through the wall assembly. The values for the interior and exterior surface resistances are respectively calculated at 20 °C and 10 °C. The thermal resistance of a homogeneous layer R_i shall be determined using equation (2), where d_i is the thickness of the layer in the element, and k_i is the thermal conductivity of the material obtained from the tabulated values in Ref. [30]:

$$R_i = \frac{d_i}{k_i} \tag{2}$$

According to the recommendations of [13]; in the case of a wall structure incorporating a well-ventilated vertical air layer, i.e., the openings between the air layer and the external environment are equal to or exceed 1500 mm^2 per meter of length in the horizontal direction, the total thermal resistance of the wall shall be obtained by disregarding the thermal resistance of the air layer and all other layers between the air layer and external environment, and including only an exterior surface resistance corresponding to the value of $R_{sur,int}$.

- In-situ measurements [23].

To measure the U-value and R-value of a wall assembly in-situ [23], describes the heat flow meter (HFM) measuring method. The test procedure requires a minimum duration of 72 h and a deviation in thermal resistance below 5% when data for the last 24 h is subtracted. These criteria would ensure convergence to an asymptotical value close to the steady-state value [31]. The data could be analyzed using the average method or dynamic method. The former method is simpler to calculate the parameters, but it needs a longer duration of measurements [23,28]. The latter method is more sophisticated compared to the former due to taking into account the thermal variations by the use of the heat equations, while it gives quality criteria of the measurement and may shorten the test duration [23,28]. The present study uses the average method to post-process the data acquired from the in-field measurements. The details on the analysis of data using the dynamic method are provided by Ref. [32].

In the average method, the U-value and R-value of the wall can be measured by using the values of the mean density of the heat flow rate and the mean temperature differences, as expressed in equations (3) and (4):

$$U_{meas} = \frac{\sum_{\tau=1}^{T} q_\tau}{\sum_{\tau=1}^{T} \left(T_{ind,\tau} - T_{out,\tau}\right)} \tag{3}$$

$$R_{wall,meas} = \frac{\sum_{\tau=1}^{T} \left(T_{wc,int,\tau} - T_{cl,ext,\tau}\right)}{\sum_{\tau=1}^{T} q_\tau} \tag{4}$$

In the aforementioned equations, index τ enumerates the time steps, q is the density of the heat flow rate per unit area, T_{ind} is the indoor temperature, T_{out} is the outdoor temperature, $T_{wc,int}$ is the temperature of the interior surface of the wall core, and $T_{cl,ext}$ is the temperature of the exterior surface of the cladding (Fig. 1). The measured R-value of the wall assembly excluding the interior and exterior surface resistances is indicated with $R_{wall,meas}$ in equation (4).

The combined standard uncertainty of measurements is calculated by taking into account the accuracy of the equipment (sensors and acquisition systems), with a coverage factor k = 2 corresponding to a 95% level of confidence [33]. The uncertainties of the U-value $u_c(U_{meas})$ and R-value $u_c(R_{wall,meas})$ are determined per equation (5) and equation (6):

$$\begin{aligned} u_c(U_{meas})^2 &= \left(\frac{\partial U_{meas}}{\partial q}\right)^2 \bullet u_c(q)^2 + \left(\frac{\partial U_{meas}}{\partial T_{ind}}\right)^2 \bullet u_c(T_{ind})^2 + \left(\frac{\partial U_{meas}}{\partial T_{out}}\right)^2 \\ &\bullet u_c(T_{out})^2 = \left(\frac{1}{T_{ind} - T_{out}}\right)^2 \bullet u_c(q)^2 + \left(\frac{-q}{(T_{ind} - T_{out})^2}\right)^2 \bullet u_c(T_{ind})^2 \\ &+ \left(\frac{q}{(T_{ind} - T_{out})^2}\right)^2 \bullet u_c(T_{out})^2 \end{aligned} \tag{5}$$

$$\begin{aligned} u_c\left(R_{wall,meas}\right)^2 &= \left(\frac{\partial R_{wall,meas}}{\partial q}\right)^2 \bullet u_c(q)^2 + \left(\frac{\partial R_{wall,meas}}{\partial T_{wc,int}}\right)^2 \\ &\bullet u_c\left(T_{wc,int}\right)^2 + \left(\frac{\partial R_{wall,meas}}{\partial T_{cl,ext}}\right)^2 \bullet u_c\left(T_{cl,ext}\right)^2 = \left(\frac{-\left(T_{wc,int} - T_{cl,ext}\right)}{q^2}\right)^2 \\ &\bullet u_c(q)^2 + \left(\frac{1}{q}\right)^2 \bullet u_c\left(T_{wc,int}\right)^2 + \left(\frac{-1}{q}\right)^2 \bullet u_c\left(T_{cl,ext}\right)^2 \end{aligned} \tag{6}$$

where $u_c(q)$ is the uncertainty of the heat flow rate measuring equipment and $u_c(T)$ is the uncertainty associated with the temperature measuring sensors.

2.2. Determination of thermal resistance of the ventilated cavity

The plausible definitions for the thermal resistance of the ventilated air-spaces behind external claddings in the steady-state condition are presented in detail by Ref. [25]. In the following paragraphs, the definitions in the transient conditions are introduced by either using a similar formulation to the steady-state condition that is also applicable in the transient analysis using the time-dependent variables (per Method 1) or by slightly modifying the steady-state formulation to adapt it to the transient analysis by considering the mean density of the heat flow rate

and the mean temperature differences through the time of the study (per Method 2).

- **Method 1: Thermal resistance**

The definition of the thermal resistance in the ventilated cavity in Method 1, i.e., *cavity thermal resistance* R_{cav}, is based on a non-linear network of thermal resistances inside the air-space. The network of thermal resistances in the cavity is formulated as shown in equation (7); using the convective transfer coefficient on each cavity surface ($h_{conv\_cl,int}$ and $h_{conv\_ins,ext}$) and radiative heat transfer coefficient (h_{rad}) between the cavity surfaces.

$$R_{cav} = \frac{\left(\frac{1}{h_{conv\_cl,int}} + \frac{1}{h_{conv\_ins,ext}}\right) \bullet \frac{1}{h_{rad}}}{\left(\frac{1}{h_{conv\_cl,int}} + \frac{1}{h_{conv\_ins,ext}}\right) + \frac{1}{h_{rad}}} \tag{7}$$

As it can be seen from equation (7), in order to determine the thermal resistance of the air gap per Method 1, the heat transfer coefficients inside the cavity should be known, which is not straightforward in practice and adds difficulties for the experimental measurements. Therefore, the thermal resistance calculation based on Method 1 is unsuitable for in-field or in-lab measurements. Consequently, it could only be used in the simulations to obtain the thermal resistance of the cavity while accepting the uncertainties due to the use of specific heat transfer correlations.

- **Method 2: Apparent thermal resistance**

The definition of the thermal resistance in the ventilated cavity per Method 2, i.e., *apparent thermal resistance* $R_{cav,app}$ (equation (8)), is defined based on the energy balance in the cavity as a function of the absolute temperature difference between the cavity surfaces ($T_{cl,int} - T_{ins,ext}$) and the heat flux through the interior surface of the wall q_{in} (Fig. 1).

$$R_{cav,app} = \frac{\sum_{j=1}^{n} \left| T_{cl,int} - T_{ins,ext} \right|}{\sum_{j=1}^{n} q_j} \tag{8}$$

The definition per Method 2 is more suitable compared to Method 1 for in-filed measurements since it only depends on the measured cavity surface temperatures and heat flux through the interior surface of the wall, which are all possible to be measured, despite its difficulty in a real application. Moreover, this method is based on the measured data and, consequently, would have more reliable results than Method 1. However, as it is presented in section 3.1, the application of Method 2 is dependent on the satisfaction of the criteria specified by the [23] to ensure a convergence of data to an asymptotical value that is close to the steady-state value. Therefore, using this method in the transient simulations is not recommended unless the results of the in-field measurements for a similar wall structure and outdoor conditions confirm that the criteria are satisfied.

Based on the above-mentioned explanations, Method 1 is employed numerically in the present study to capture the dynamic behavior of the thermal resistance of the cavity under transient conditions. The results of the numerical analysis are provided in section 3.1. The definition per Method 2 is used to experimentally determine the thermal resistance of the ventilated cavity in a wall structure of a test facility, and the results of the in-field measurements are presented in section 3.2.

2.3. Numerical simulations

The multi-layer ventilated wall assembly is numerically modeled in MATLAB® employing a finite-difference method. The procedure used for simulating the problem is elaborated by Ref. [12]. The system is modeled as a two-dimensional nodal network with 5 nodes along with the height and 3 nodes through the width of the geometry. The simulations for each day of interest are performed using 32 h of weather data that includes 8 h prior to the chosen day (16:00–00:00) to ensure the stability of the model (results for 8 prior hours are not considered). It is assumed that the flow across the width of the air cavity is fully developed, the materials across the entire layer have constant properties with no infiltration through the photovoltaic wall section and the building materials, and the thermal bridges caused by the studs, junctions, and connections are negligible. It should be mentioned that the computational model is validated for ventilated walls with both passive and active façades using experimental measurements [12]. The heat transfer correlations used to determine the thermal resistance of the cavity, the case study scenarios, and the weather data used for the simulations are described in the following paragraphs.

- Heat transfer correlations

According to the explanations provided in section 2.2, the convective and radiative heat transfer coefficients in the cavity should be known to numerically analyze the thermal resistance of the ventilated cavity using Method 1 per equation (8). Therefore, the radiative heat transfer coefficient between the cavity surfaces is expressed by equation (9) considering the simplified linearized calculations [34], which is a function of the cavity surface temperatures ($T_{cl,int}$ and $T_{ins,ext}$) and their emissivity ($\varepsilon_{cl,int}$ and $\varepsilon_{ins,ext}$) (Fig. 1):

$$h_{rad} = \frac{\sigma \bullet \left(T_{cl,int}^2 + T_{ins,ext}^2\right) \bullet \left(T_{cl,int} + T_{ins,ext}\right)}{1/\varepsilon_{cl,int} + 1/\varepsilon_{ins,ext} - 1} \tag{9}$$

The convective heat transfer coefficients within the air channel are categorized depending on the convection mode and the flow regime in the channel. The type of convection, i.e., natural, forced, or mixed, is specified and the flow in each convection mode is distinguished between the laminar and turbulent regimes. The detailed description of the correlations used in the numerical model to obtain the convective heat transfer coefficients is elaborated by Ref. [12]; thus, it is not repeated in this paper.

- Case study scenarios

The aim of the numerical simulations in the present study is to compare the thermal resistance of the ventilated wall assemblies having passive and active cladding systems considering two values for the thickness of the air gap to study the effect of both narrow and wide cavities behind the traditional and BIPV façades [12]. The schematic representation of the wall assemblies simulated in this study is shown in Fig. 2. The use of wood has increased over the past decades due to its sustainability and environmental qualities [35]. Therefore, the timber hardwood with a typical thickness of 100 mm suggested by Swisspor [50] is selected as the load-bearing layer in the wall core. The inner side of the load-bearing wall is protected by a 10 mm fiber plasterboard. The U-value for the wall assembly is fixed equal to 0.16 ($W/m^2 \bullet K$) to comply with the Swiss building code SIA 380/1, which requires 0.17 ($W/m^2 \bullet K$) for the opaque façades of new buildings. The thickness of the insulation, equal to 160 mm, is determined by fixing the thickness of the layers of the wall assembly (excluding insulation) and following the procedure described in section 2.1 using the thermo-physical properties of the materials listed in Table 1. The thickness of the air gap behind the external cladding is considered as 45 mm and 110 mm. The selected two values represent the presence of both thin and thick cavities behind the traditional and BIPV façades. The former is recommended for a passive ventilated façade to reduce the heat gain/loss through the wall, and the latter is the optimal width to minimize the PV overheating [12]. The presence of reflective insulation attached to the cavity wall adjacent to the wall core is also modeled to compare the impact of the low emissivity

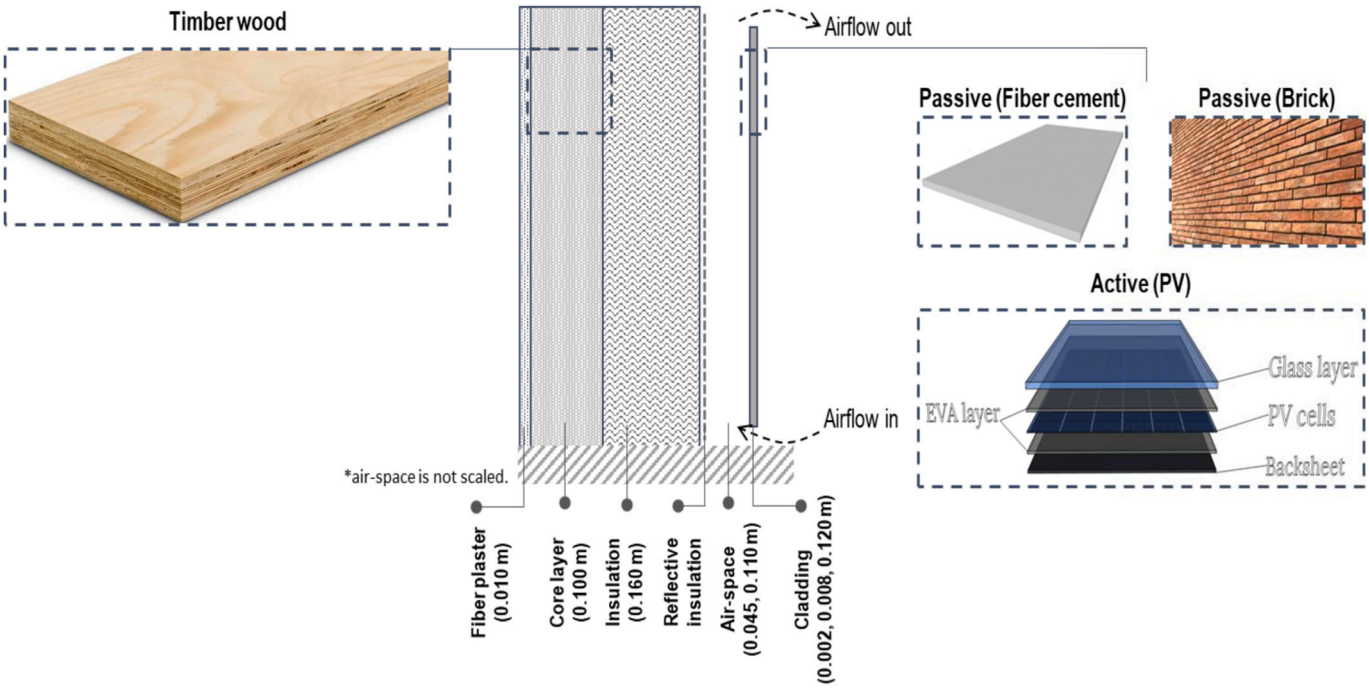

Fig. 2. Different ventilated wall assemblies simulated (refer to Table 1 for more information on the thermo-physical properties of each layer).

Table 1
Properties of the wall layers modeled [36,37].

Parameter	d	k	ρ	c_p	R-value	ε	α	τ
Unit	m	W/(m • K)	kg/m^3	J/kg·K	m^2•K/W	[−]	[−]	[−]
Active facade (PV)*								
Tempered glass	0.0036	1.8	3000	500	0.002	0.88	0.10	0.90
EVA film	0.0004	0.35	960	2090	0.001	–	–	–
PV cells	0.0004	148	2330	700	≈ 0	–	0.90	–
Back sheet	0.0004	0.13	1450	1650	0.003	0.87	0.90	–
Passive facade								
Fiber cement (FC)	0.008	0.58	1900	1000	0.01	0.90	0.70	–
Brick (Br)	0.120	0.43	1200	900	0.28	0.93	0.6	–
Wall core								
Reflective insulation (ε)	0.0002	235	2700	890	≈ 0	0.05	0.04	–
Insulation	0.160	0.03	25	1380	5.33	0.90	–	–
Timber wood	0.100	0.14	400	1255	0.71	–	–	–
Fiber plaster	0.010	0.18	837	800	0.06	0.90	–	–
Air cavity (45, 110)	0.045, 0.110	varies**	varies	varies	–	–	–	–

* Abbreviations are provided in parenthesis. ** The air properties vary as a function of the air temperature.

and high emissivity cavity surface on the thermal resistance of the ventilated air gap.

Two types of the passive facade are selected, a fiber cement board and a brick wall, to represent the traditional claddings with different thermo-physical properties. To model the BIPV system as the active façade, the traditional cladding is replaced by a typical polycrystalline photovoltaic module. The height of the active façade is considered equal to the height of a standard PV module, i.e., 1.64 m [38], which can cover a large part of the wall in a single-story building. The reason for choosing this height is to exclude the effects of airflow movement within the open joints between the PV panels, which could have a considerable impact on the hydrodynamic behavior of the airflow in the ventilated air gap and, consequently, on the results of the simulations. A similar height for the walls with passive claddings is considered to make the results comparable with the active façade. In total, 24 scenarios are simulated by considering combinations of different variables, including the cladding type, outdoor conditions, cavity thickness, and absence/presence of reflective insulation on the cavity surface. Different cases simulated in this study are abbreviated in the hereafter text by assigning the letters provided in parenthesis in Table 1 to represent the condition of the case study. For instance, Br-ε indicates the case study of the wall with passive Brick cladding (Br) cladding and the presence of reflective insulation (ε) on the cavity surface adjacent to the wall core (in the case of the absence of reflective insulation, no abbreviation is used). The outdoor condition is also abbreviated for the Summer (S) and Winter (W) scenarios.

- Weather data

The effect of seasonal variation is investigated in this study considering typical days in the summer and winter of 2019 using the weather data measured at 5-min intervals in Lausanne, Switzerland [39], which represents a temperate oceanic climate (i.e., Cfb) specified by Ref. [40]. Following the procedure described by Ref. [12]; the typical representative days in summer and winter are selected as August 13th and December 14th of 2019, respectively. The horizontal solar radiation measured by the weather station is converted to the vertical direction to align with a west-oriented façade [41]. Indoor air temperatures are assumed to be 21 °C in winter and 26 °C in summer (SIA 2024:2015

[49]). The diurnal variations of outdoor air temperature, vertical solar radiation, and wind speed are shown in Fig. 3.

2.4. Experimental measurements

To experimentally measure the thermal resistance of the ventilated air-space and the total R-value of the entire assembly, in-field measurements are carried out in a test facility. The former is measured following Method 2 (section 2.2), and the latter is obtained using recommendations provided in the [23]. In the next sections, the research facility, the layout of the sensors installed, and the monitored outdoor environment are described.

- Research facility

The on-site measurements are performed in a research facility (Fig. 4a) called CELLS (Controlled Environment for Living Lab Studies) in the Smart Living Lab located in Fribourg, Switzerland. The facility is composed of two rooms almost identical in size but with different thermal inertia walls (Fig. 4b). The room with low inertia walls is East-oriented that is separated by a technical space from the West-oriented room with high inertia walls. The envelope of the test facility is exposed to the exterior with natural outdoor conditions, and the interior space is mechanically conditioned. The South and North facades of the test facility have two external windows each, while the East and West facades are fully opaque with wooden external claddings. The external façade of the wall structure is separated from the wall core with horizontal and vertical battens that create an air-space behind the cladding. The cavity is naturally ventilated by the airflow that can freely move through the bottom and top openings. The thermo-physical properties and the design R-value (equation (2)) of the layers used in the wall assembly are summarized in Table 2.

- Wall layout and sensor installation

The schematic of the sensors installed on different parts of the East-oriented wall is depicted in Fig. 4c. A similar configuration can be considered for the West-oriented wall with extra layers on the interior side. The temperature on each layer is monitored by using thermocouples (T-type with the accuracy of $\pm 0.2\ ^{\circ}C$, calibrated prior to the measurements) installed on the exterior and interior surfaces of the cladding, within the air-space, on the exterior surface of the insulation that is adjacent to the cavity, and on the interior surface of the wall core in the room. The U-value and R-value of the walls are measured following the guidelines provided in ISO 9869–1:2014 using data from different positions; three sensors are distributed in the center along with the height of each surface. In addition to the surface temperatures, the indoor and outdoor air temperatures adjacent to the interior and exterior surfaces are measured using thermocouples attached at a 10 cm distance to the wall surface [32]; Rahiminejad and Khovalyg 2022b). The outdoor air temperature sensors are shielded from direct solar radiation and ventilated [23]. To measure the heat flux through the interior surface, three heat flux sensors (HFP01, Hukseflux) on each wall of the test facility are used with an accuracy of ±6% and different sensitivities ranging from 58.01 μV/(W/m^2) to 61.96 μV/(W/m^2). The sensors are attached to the interior surface of the walls aligned with the temperature sensors on the center line, as this is the most thermally stable area [23,27]. The data of all sensors are continuously recorded at 1-min intervals with a centralized data acquisition system (DAQ 34972 A, Keysight) connected to a PC.

- Outdoor environment monitoring

Two sets of outdoor environmental sensing equipment, one installed on each façade of the test facility (Fig. 4a), are used to measure the outdoor conditions adjacent to the walls. The equipment consists of an air temperature sensor (S-THB-M002, Onset), Davis® wind speed and direction sensor (S-WCF-M003, Onset), and a silicon pyranometer for global horizontal irradiance (S-LIB-M003, Onset). The sensors are connected to two micro station data loggers (H21-USB, Onset), which are configured to record data at 1-min intervals. The experimental campaign was conducted from the 23rd of December 2020 to the 10th of January 2021. The diurnal variation of outdoor conditions measured in this period is shown in Fig. 5. It should be noted that the instruments for environmental sensing are placed on the facades to monitor the local microclimate around the test facility with high accuracy [42].

3. Results

3.1. Numerical simulations

The results of the numerical simulations are provided in this section. First, the U-value and R-value of the wall assembly considered in the numerical model are calculated. Second, the results of the thermal resistance of the ventilated air-space under various conditions are presented. Thereafter, the static R-value of the wall obtained from the [13] standard is compared with the results of simulations. Moreover, the detailed analysis of the correlations between the thermal resistance of

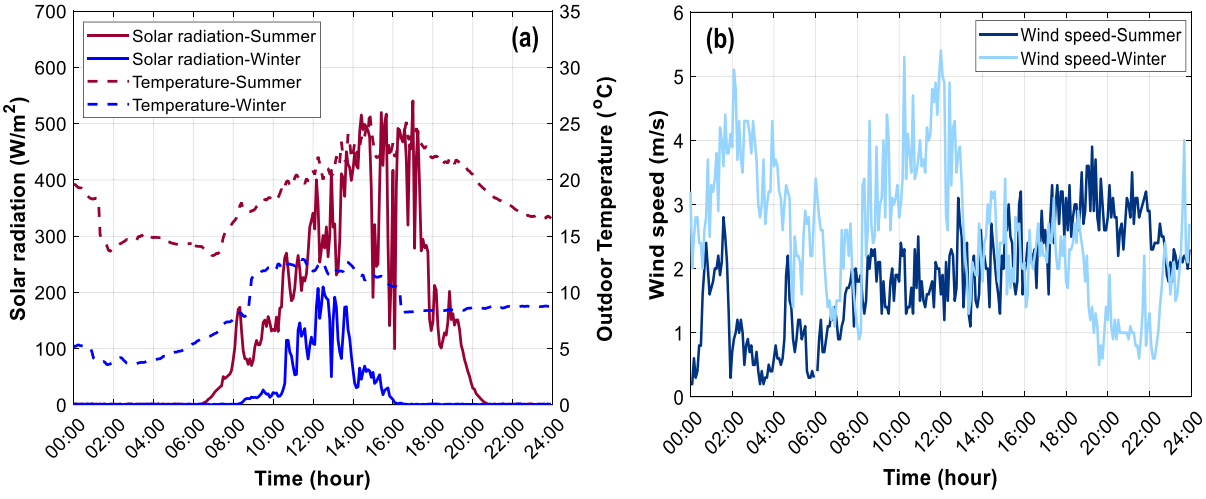

Fig. 3. Outdoor conditions for representative days in summer and winter (August 13th and December 14th of 2019) (a) outdoor air temperature and vertical solar radiation (b) wind speed.

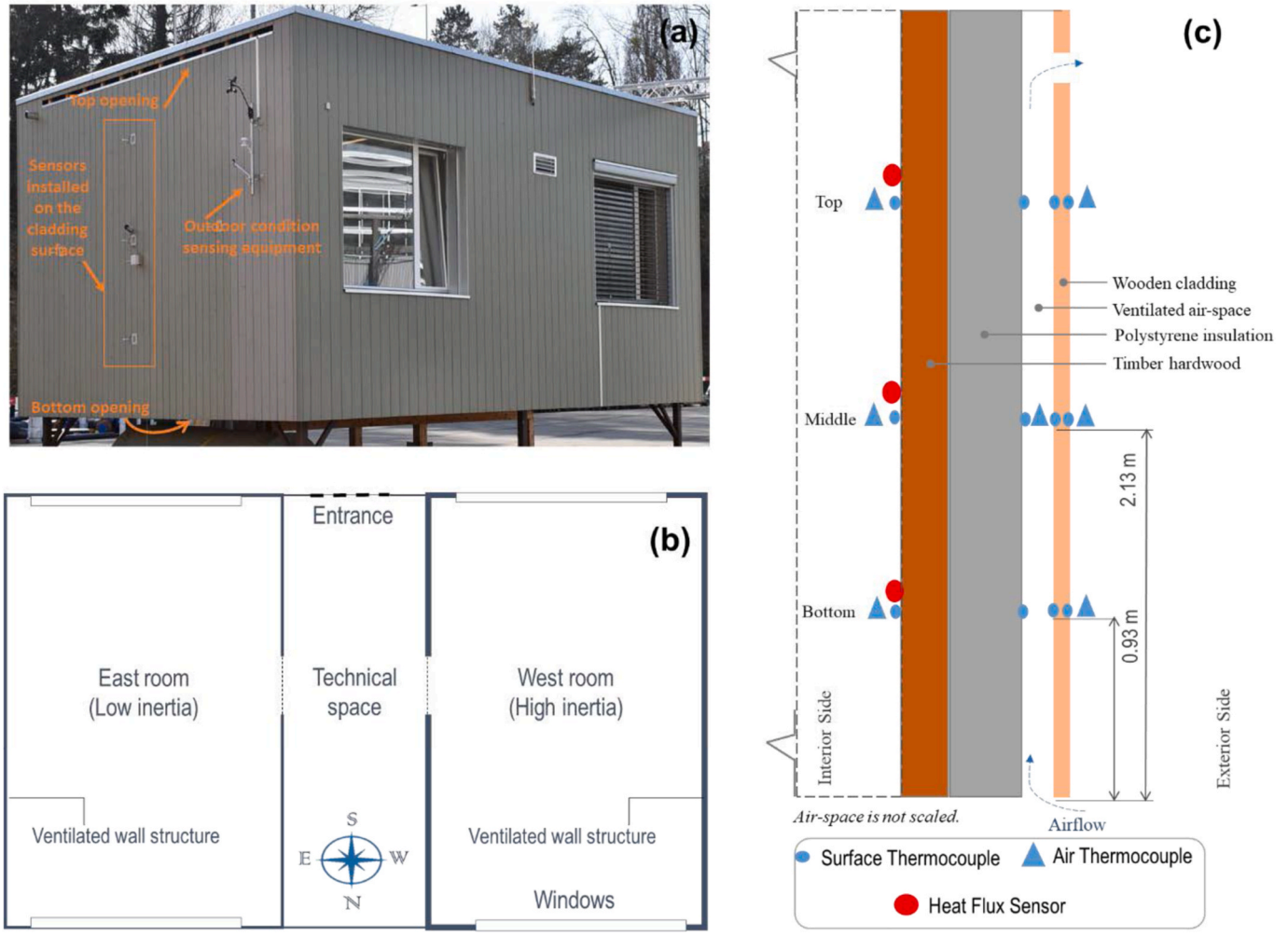

Fig. 4. (a) Outside view of the test facility, (b) floor plan of the test facility, (c) Cross-section schematic of the sensors installed on different surfaces of the East-oriented wall (a similar configuration is set up for the West wall).

Table 2
Properties of the ventilated wall structures of the test facility [12].

Material (exterior to interior)	d (m)	k (W/m•K)	ρ(kg/m^3)	c_p (J/kg•K)	R-value (m^2•K/W)
Wooden cladding	0.024	0.10	450	1800	0.24
Air cavity	0.070	0.03*	1.20*	1.01*	–
Expanded polystyrene insulation	0.180	0.03	15	1404	6.00
Timber hardwood	0.140	0.13	471	1600	1.08
Earth brick**	0.050	0.79	1900	1100	0.06
Jute coating**	0.015	0.80	1600	1450	0.02

* The air properties are specified at 20 °C. ** Additional layers of the West wall.

the cavity and some influential parameters is performed in this section.

- U-value and R-value of the ventilated walls

According to the description of the wall assembly for the numerical simulations in section 2.3, the designed U-value of the wall structures $U_{des,sim}$ is fixed equal to 0.16 (W/m^2•K); therefore, according to equation (1), the total designed R-value of the wall $R_{tot,des,sim}$ becomes equal to 6.25 (m^2•K/W). Considering the descriptions provided in section 2.1, the R-value of a wall, including a well-ventilated air layer, shall be obtained by excluding the thermal resistance of the air layer and all other layers between the air layer and external environment and considering an exterior surface resistance equal to 0.13 (m^2•K/W). Consequently, the designed R-value of the wall assembly, excluding the interior and exterior surface resistances $R_{wall,des,sim}$ would be equal to 5.99 (m^2•K/W).

- Thermal resistance of the ventilated cavity

The results of the thermal resistance of the ventilated cavity are provided in this section, following the definition per Method 1 (section 2.2). The values of R_{cav} for the walls with passive claddings (brick and fiber cement) and active façade (BIPV) are determined. The results are provided for the ventilated cavities with a thickness of 45 mm and 110 mm. The effect of the reflective insulation on the cavity surface adjacent to the wall core on the results is also considered. Moreover, this section presents the profiles of temperature distribution through the wall assembly and airflow speed in the cavity to have a better physical interpretation of the results.

The plots of R_{cav} for different simulated scenarios are shown in Fig. 6. The results reveal that the thermal resistance of the ventilated cavity obtained per Method 1 dynamically varies during the day, which is attributed to the change in the heat transfer coefficients inside the airspace (equation (7)). This change is due to the variation of the thermo-hydrodynamic characteristics of the airflow in the cavity including its speed and temperature. Consequently, the cavity surface temperatures change, and the heat transfer coefficients vary during the day. All of these observations are caused by the diurnal variation of the

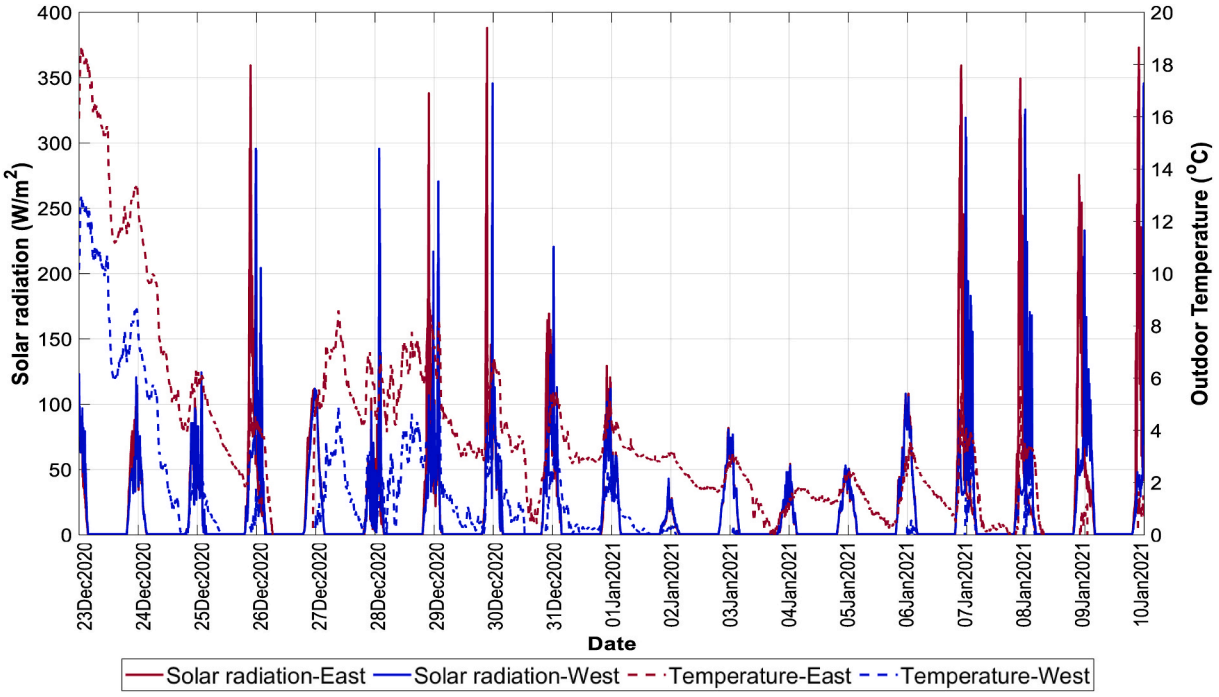

Fig. 5. Outdoor temperature ($^{\circ}C$) and solar radiation (W/m^2) measured on the façades of the test facility.

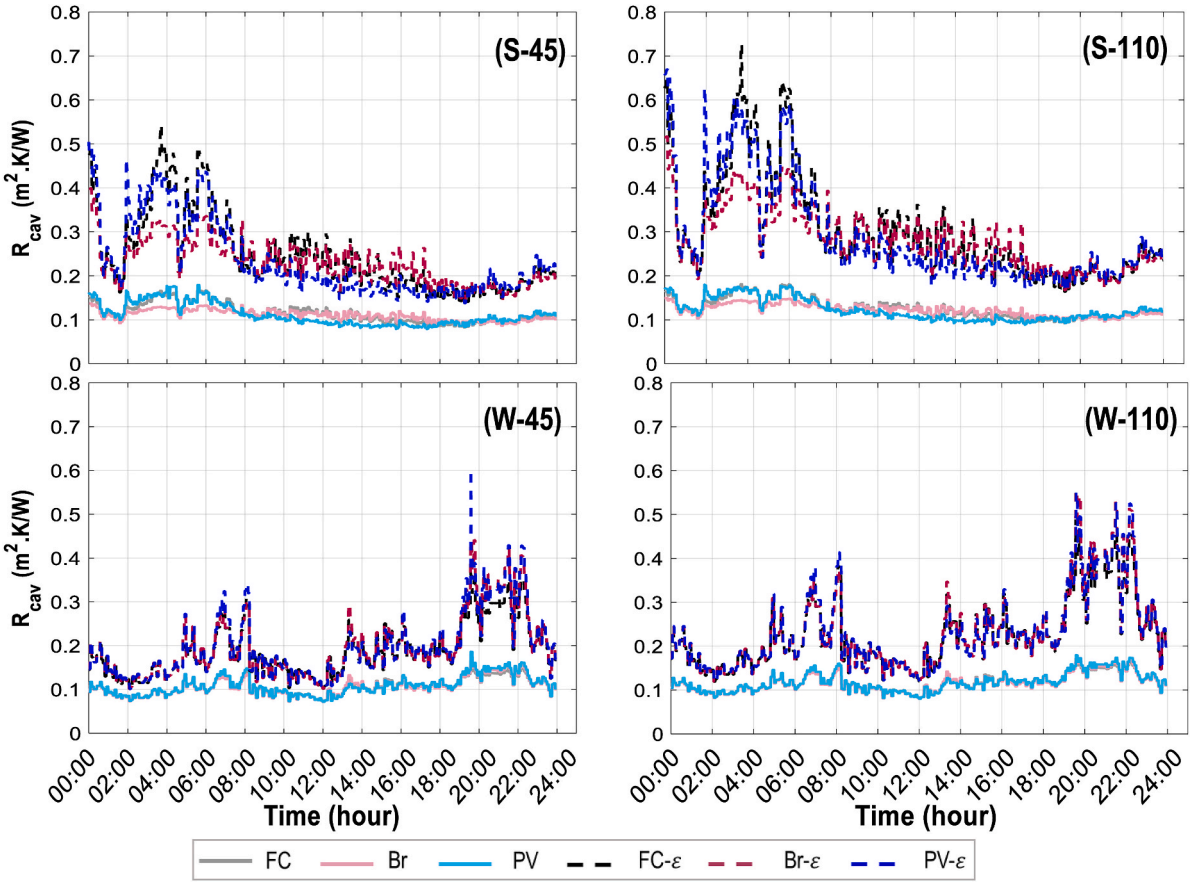

Fig. 6. Profiles of the thermal resistance of the ventilated cavity simulated for different wall structures (refer to Table 1 for abbreviations).

outdoor conditions, as presented in Fig. 3. According to equation (7), the definition of R_{cav} per Method 1 is a non-linear function of the airflow speed, its temperature, and the cavity surface temperatures. Therefore, the effect of the change in the temperature and airflow rate in the air gap on the behavior of R_{cav} is a complex phenomenon and cannot be simply predicted.

Based on the results, altering the cladding type could affect the dynamic variation of R_{cav} during a day. According to the plots, the thermal resistance of the ventilated cavity behind the brick cladding is lower compared to the other claddings from 2:00 to 8:00 in summer, mainly due to the higher temperature of the interior surface of cladding during this period (Fig. 7). This behavior is changed in the middle of the day from 10:00 to 17:00 when solar radiation is increased, and the temperature of the interior surface of the cladding has become lower in the brick wall compared to the other claddings. Therefore, the radiation heat transfer inside the air-space is reduced and R_{cav} is increased. The results reveal that replacing passive claddings with an active BIPV façade has a more considerable effect on R_{cav} in summer compared to winter. This could be due to the presence of the high solar flux in the former, which increases the temperature of the cavity surfaces (Fig. 7),

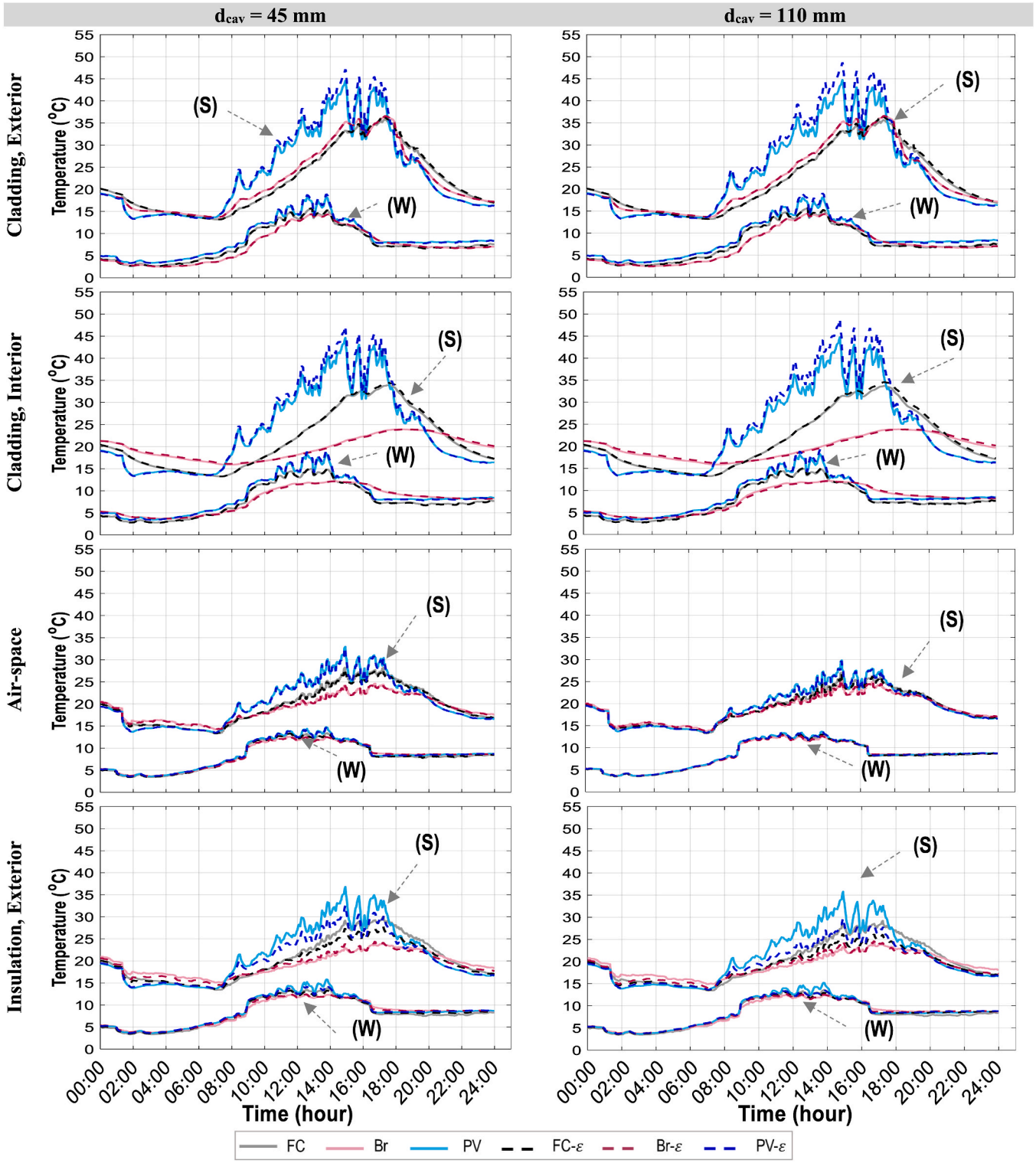

Fig. 7. Temperature profiles at the middle point on different surfaces in the wall structure (refer to Table 1 for abbreviations). Summer cases (S) are upper curves, and winter cases (W) are lower curves.

and, consequently, results in a lower R_{cav} in the BIPV system during the day time. The results in Fig. 6 reveal that the amplitudes of R_{cav} become lower in winter compared to summer. Considering the plots shown in Fig. 7, it can be seen that the temperature in the cavity is lower in winter than in summer. However, the airspeed in the former is higher (Fig. 8), which has eventually reduced the thermal resistance of the ventilated cavity in winter. The results also show that the difference between R_{cav} of different cladding types is negligible in winter and the profiles are most of the time overlapped in this condition. This could be attributed to the temperature profiles (Fig. 7) and the airflow speed in the cavity (Fig. 8), which are relatively similar for all cladding types. Moreover, comparing the values of R_{cav} between the cases with and without reflective insulation on the cavity surface adjacent to the wall core, the plots in Fig. 6 show that the difference becomes lower in winter compared to summer. This is due to the lower temperature difference between the two cases on the exterior surface of insulation in the wintertime (Fig. 7).

The results in Fig. 6 show that increasing the cavity thickness from 45 mm to 110 mm could increase R_{cav}, which is more pronounced in the summer representative day for the cases with reflective insulation in the cavity. As shown in Fig. 7, the increase in the cavity thickness reduces the temperature of the interior surface of cladding, the airflow temperature in the air-space, and the exterior surface of the insulation. These observations are due to the slight increase in the airspeed in the cavity with a higher thickness (Fig. 8). According to the results shown in Fig. 6, despite expecting a reduction in the thermal resistance of the ventilated cavity due to an increment in the airspeed in the air gap [25], the results indicate that R_{cav} is decreased at the air-space with a higher thickness, which could be attributed to the decrement in the temperature profiles in the cavity. The change in the behavior of the thermal resistance of the air-space by varying the thickness of the cavity, which is caused by the change of the heat transfer coefficients inside the air gap, is also reported by Refs. [18,21] for a non-ventilated air-space in the wall assembly. Based on the results presented in Fig. 6, the values of R_{cav} become higher in case of the presence of the reflective insulation on the cavity surface adjacent to the wall core (exterior surface of insulation). The value of R_{cav} changes between 0.09 and 0.2 (m^2•K/W) in the case of the absence of the reflective insulation, while it varies between 0.15 and 0.75 (m^2•K/W) if the reflective insulation is used. This observation is attributed to the impact of the lower emissivity of the reflective insulation on the temperature distribution on the cavity surfaces as shown in Fig. 7. Therefore, using a thin layer of reflective insulation on the cavity surface could significantly increase the thermal resistance of the ventilated air-space behind external claddings. Similar behavior is observed in the literature for a non-ventilated air gap in the wall assembly, where the impact of the lower emissivity of the cavity surface on increasing the thermal resistance of the enclosed air-space is reported [16,17]; Meyer et al., 2109; [18].

The profiles of the total thermal resistance of the wall structures R_{tot} are presented in Fig. 9. The results are shown for two cases; the design value calculated in section 2.1 based on the recommendations provided in Ref. [13]; and the design values including R_{cav} obtained from the numerical simulations described in section 3.1. For both cases, the values are determined using equation (1); in the former, a static value is assigned for the thermal resistance of the ventilated cavity, while in the latter, the dynamic change of R_{cav} is taken into account. The results reveal that R_{tot} becomes different when the external cladding is changed. This is partially due to the difference in the R_{cav}, as it was shown in Fig. 6, and partially due to the impact of the change in the façade on the performance of the wall structure. This effect is also reported by Refs. [21,22]; where the change in the external cladding has caused a difference in the R_{tot} measured. Moreover, based on the results, the total thermal resistance of the wall structure is always higher than the design value determined by the standard. The minimum and maximum differences between the two values are equal to 0.15 (m^2•K/W) and 0.75 (m^2•K/W), respectively, which are 2.5% and 12% higher than the static value of 6.25 (m^2•K/W). A similar observation is reported by Ref. [3]; where the total thermal resistance of the ventilated wall assembly is shown to be 7% higher than the theoretical value obtained following [13]. Therefore, the results confirm that the static value obtained from the recommendations provided in the [13] yields the minimum total R-value required for the wall assembly. Consequently, it could be safely used for designing opaque ventilated wall structures, although the dynamic change of R_{tot} could be captured with a higher accuracy using the procedure described in this study.

The scatter plots of R_{cav} obtained using Method 1 versus the solar radiation and outdoor temperature are shown in Fig. 10. The results reveal that R_{cav} becomes lower when the solar radiation is high, i.e., R_{cav} is the highest at nighttime when the Sun is not present. This is due to the impact of the solar flux on the airspeed in the ventilated cavity. The higher the solar radiation, the higher the temperature and airspeed in the cavity, and consequently, the lower the thermal resistance of the

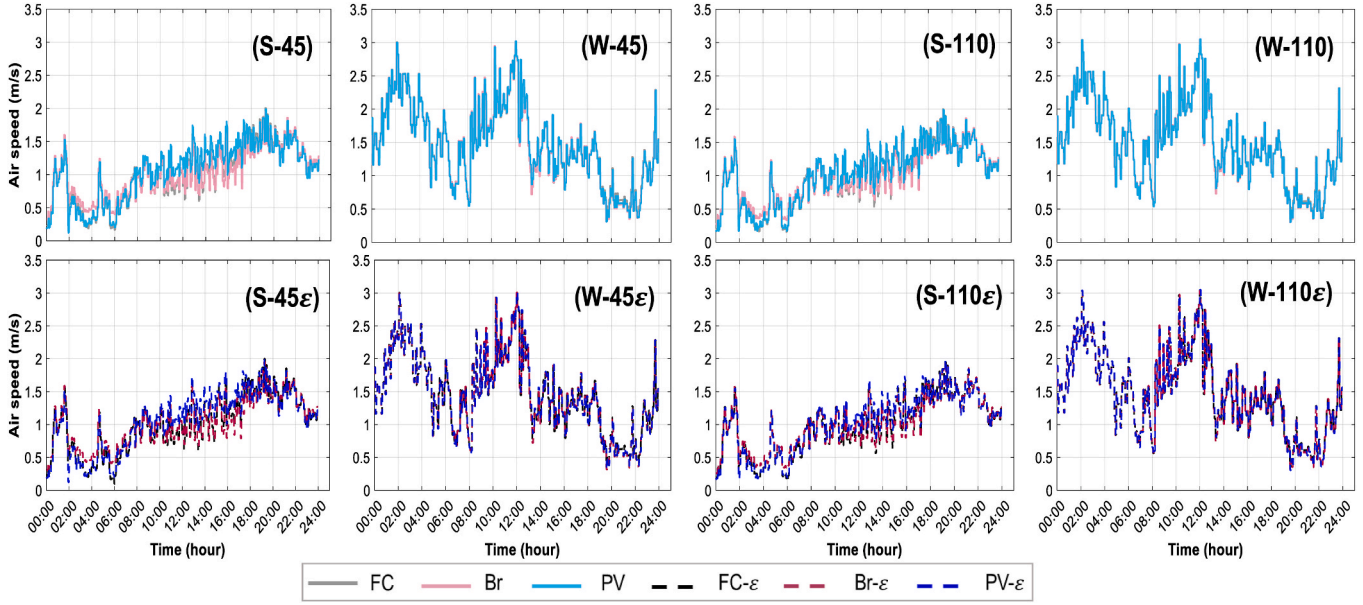

Fig. 8. Profiles of the airspeed at the middle point in the air-space (refer to Table 1 for abbreviations).

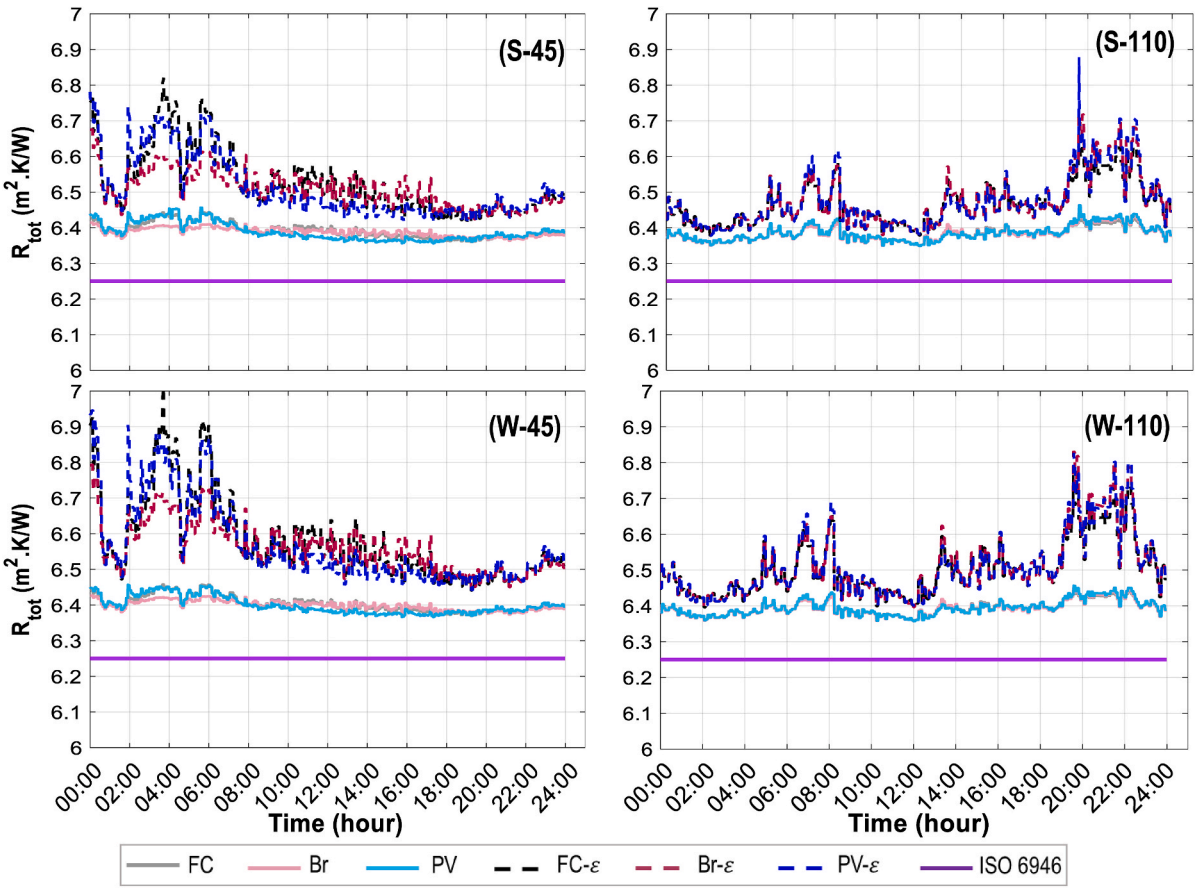

Fig. 9. Profiles of the design and dynamic total thermal resistance of the wall structures simulated (refer to Table 1 for abbreviations).

ventilated cavity becomes [25]. Considering the plots of R_{cav} versus the outdoor temperature, it can be seen that the increase in the outdoor temperature causes a decrement in R_{cav} in the summertime, while in the wintertime, the pattern is not clear, and it seems that there is no correlation between these two parameters. Moreover, the results show high values of R_{cav} at some specific outdoor temperatures, i.e., at 14 $^{\circ}C$ and 19 $^{\circ}C$ in summer and in at 8 $^{\circ}C$ winter. According to the outdoor conditions shown in Fig. 3, the aforementioned temperatures occur between 00:00 to 07:00 in summer and between 16:00 to 24:00 in winter, when the solar radiation is not present and the wind speed is low. Consequently, the air speed in the cavity decreases, and the thermal resistance of the air-space increases.

The correlations between R_{cav} and the airflow characteristics inside the air gap are further analyzed in Fig. 10. According to the results, the value of R_{cav} decreases when airspeed in the cavity increases. This is due to the higher convection heat transfer between the airflow in the air-space and the cavity surfaces, which consequently reduces the thermal resistance of the air gap determined per Method 1 (section 2.2). Moreover, the results indicate that the increment in the airspeed has a higher effect on R_{cav} when reflective insulation is used in the air-space, i.e., the slope of the curve is steeper in this case. The reason is the higher temperature difference between the cavity surfaces in case of the presence of the reflective insulation, which affects the radiation heat transfer coefficient used in equation (7), and, therefore, reduces the values of R_{cav} with a greater inclination. Considering the relationship between R_{cav} and cavity temperature, the results in Fig. 10 show that, generally, the former is reduced at higher values of the latter in summer. However, the results in winter show no clear correlation between the two parameters, which is due to the dependence of the cavity temperature on the outdoor temperature; thus, the sudden increase in the values of R_{cav} at some specific cavity temerpatures could be justified with a similar reason explained for the outdoor temperature.

3.2. Experimental measurements

In this section, first, the U-value and R-value of the ventialted walls in the test facility are determined using the procedure described in the [13,23] standards. Thereafter, the thermal resistances of ventilated cavities behind external claddings of the test facility are obtained per Method 2 following the procedure described in section 2.2.

- U-value and R-value of the ventilated walls

3.2.1. Design calculations

Based on the thermo-physical properties of the East and West wall structures of the test building (Table 2), the design U-value and R-value of the ventilated walls could be calculated following the procedure described in section 2.1. Therefore, the total design R-value $R_{tot,des,exp}$ of the East and West-oriented walls become respectively equal to 7.14 (m^2•K/W) and 7.22 (m^2•K/W), which alternatively means that the design U-value $U_{des,exp}$ of the East and West-oriented walls are respectively equal to 0.140 (W/m^2•K) and 0.138 (W/m^2•K). Moreover, the design R-value of the walls $R_{wall,des,exp}$, obtained by excluding the surface resistances from $R_{tot,des,exp}$, is equal to 6.88 (m^2•K/W) for the East and 6.97 (m^2•K/W) for the West wall.

3.2.2. In-situ measurements

As described in section 2.4, the experimental campaign is carried out over 18 days from the 23rd of December 2020 to the 10th of January 2021. The measurements are performed for 3 positions along with the height of the ventilated wall structures of the test facility with the East

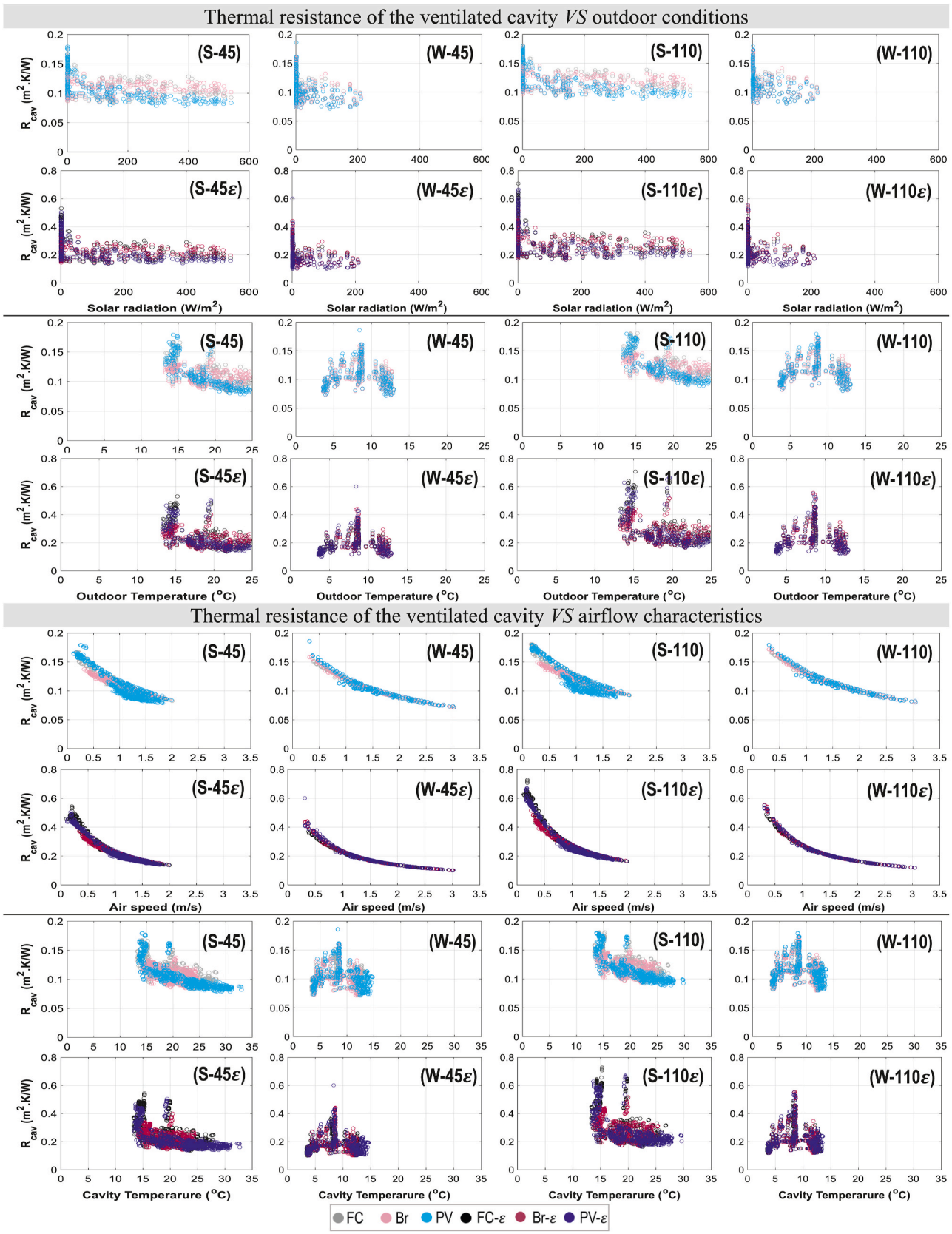

Fig. 10. Scatter plots for the thermal resistance of the ventilated cavity versus outdoor conditions and airflow characteristics (refer to Table 1 for abbreviations).

and West orientations. The plots of the outdoor air temperature T_{out}, indoor air temperature T_{ind}, exterior surface temperature of the wall $T_{cl,ext}$, interior surface temperature of the wall $T_{wc,int}$, and the heat flux through the interior surface of the wall q_{in} are shown in Fig. 11.

According to the plots, the temperature difference between the indoor and outdoor spaces is always higher than 10 °C, which complies with the recommendations specified in Ref. [23]. Moreover, as the experiment has been carried out over 18 days, the minimum duration (72 h) required for the measurements is fulfilled [23]. Comparing the temperature of a wall along with the height, the plots in Fig. 11 reveal that the values are slightly different, mainly due to the buoyancy effect and wind effect that cause a temperature distribution at different positions of the ventilated wall assembly. According to the data measured, the heat flux leaving the interior surface of the East wall is higher than the corresponding value in the West wall, which was expectable due to the lower thermal mass of the former wall.

The results shown in Fig. 11 are analyzed following the procedure described in section 2.1 to determine the thermal transmittance and thermal resistance of the wall assemblies. The plots of the measured U-value $U_{meas,exp}$ and the wall's R-value $R_{wall,meas,exp}$ are depicted in Fig. 12. The results are presented for the 3 positions along with the height of the wall and the corresponding averaged value (solid lines in the plots). It should be noted that according to the data processing, the criteria specified in the [23] regarding the R-value deviation from the last 24 h no more than 5% are satisfied.

Based on the results, the values of $U_{meas,exp}$ and $R_{wall,meas,exp}$ of the East wall are respectively lower and higher compared to the West wall, which is attributed to the additional layers used in the latter wall to increase its thermal inertia. Moreover, the results reveal that the measured values slightly vary in different positions along with the height of the wall, which is caused by the difference in the temperatures and heat flux values presented in Fig. 11. The impact of the sensor position on the variation of the U-value results in the in-field measurements is also reported by Sang-Tae and Jeong (2019). The converged values in Fig. 12 and the difference between the average value and the design value are shown in Table 3. According to the results, the average U-value measured for the walls is increased by almost 10% comparing the East and West-oriented walls. The results also indicate that the difference between the design and measured (averaged) U-value of the wall reaches 8.57% for the East and 0.72% for the West wall. The corresponding differences in the R-value of the walls are respectively 6.40% and 0.86% for the East and West walls of the test facility. Therefore, the errors obtained in the West wall are lower compared to the East wall, which could be attributed to the higher thermal mass of the former that causes a more stable temperature gradient on the interior side of the wall [12]. The reason for the discrepancy between the design calculation and the measured value is mainly due to the inaccurate values of the thickness and thermal conductivity of the walls used in the calculations (equation (2)), which has also been reported in the literature [43]. observed a difference of 8.1% and 18.9% in the U-value analysis of a ceramic wall with a differential environmental temperature respectively equal to 10 °C and 7 °C. The difference between the theoretical and the measured

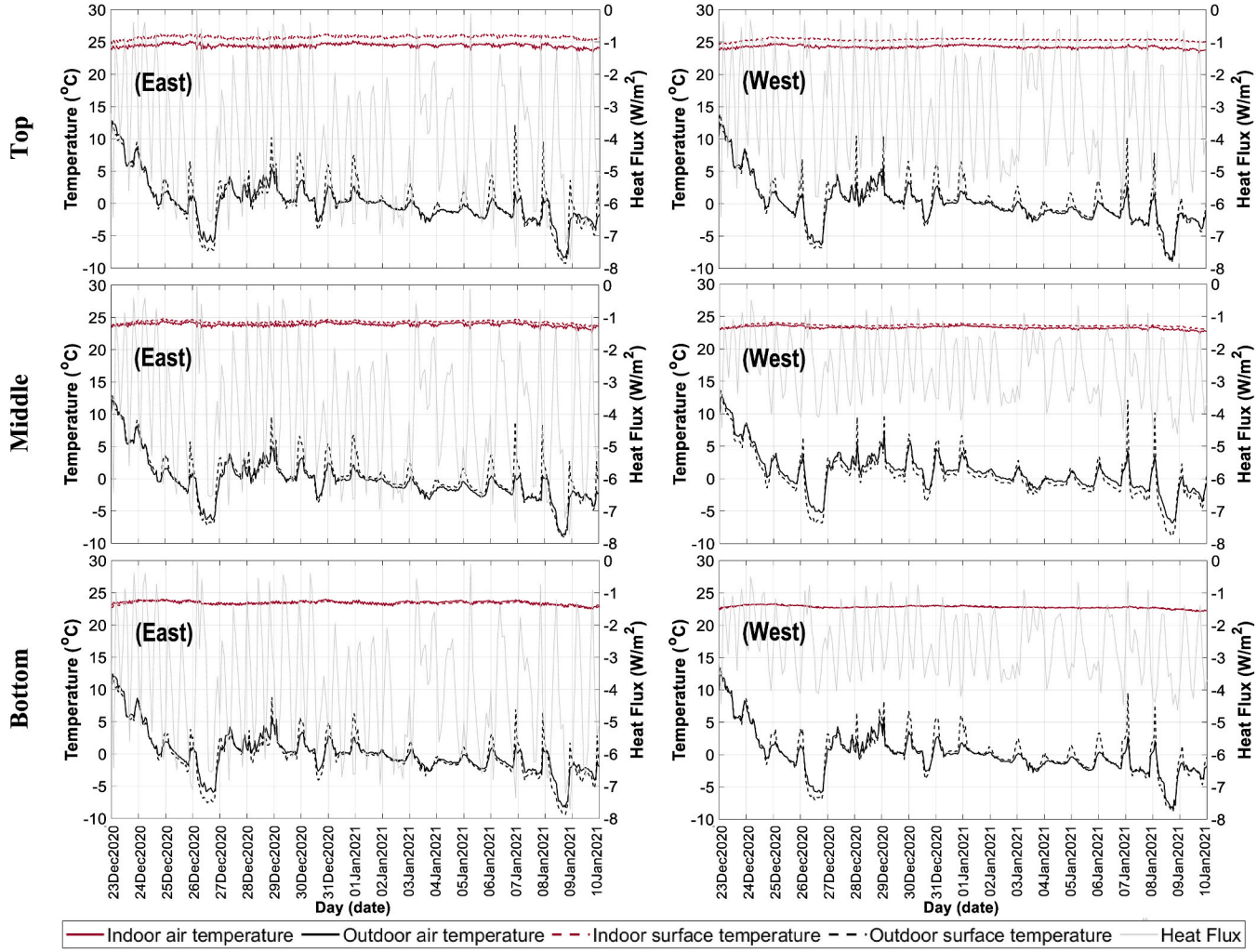

Fig. 11. Temperature (°C) and Heat flux (W/m^2) measured for the East and West walls of the test facility.

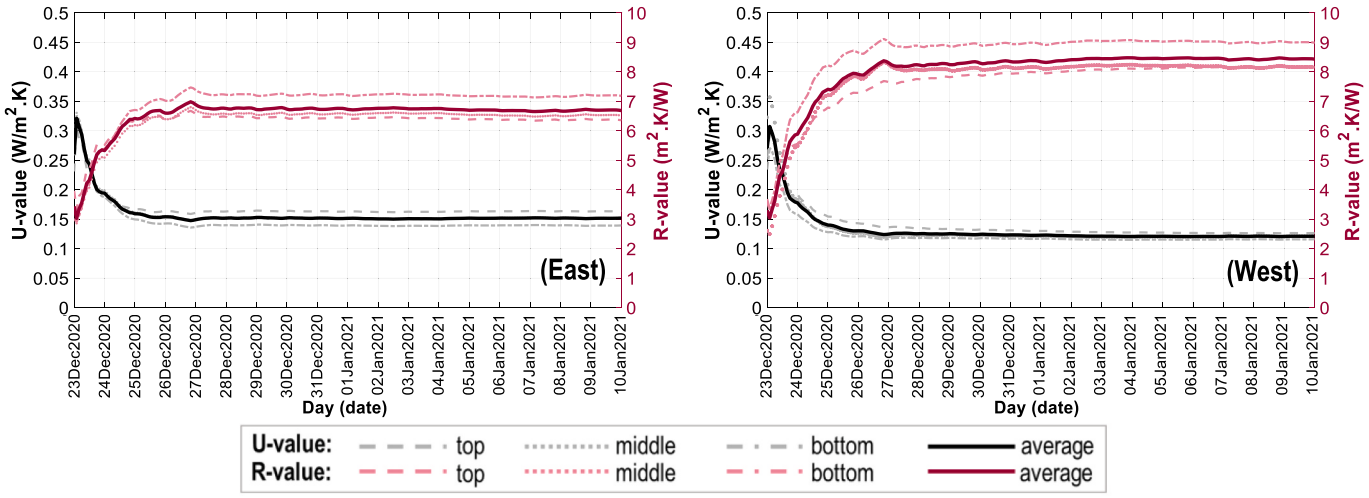

Fig. 12. The U-value and R-value measured for the East and West walls of the test facility.

Table 3
The design and measured U-value and R-value for the East and West walls of the test facility.

Wall	U-value (W/m^2•K)					
	Design $U_{des,exp}$	Measurement $U_{meas,exp} \pm u_c$				$\frac{\lvert U_{meas,exp,ave} - U_{des,exp}\rvert}{U_{des,exp}} \times 100$
		Top	Middle	Bottom	Averaged	
East	0.140	0.164±0.016	0.152±0.016	0.139±0.014	0.152±0.015	8.57
West	0.138	0.145±0.06	0.139±0.07	0.133±0.08	0.139±0.07	0.72
Wall	**R-value (m^2•K/W)**					
	Design $R_{wall,des,exp}$	**Measurement** $R_{wall,meas,exp} \pm u_c$				$\frac{\lvert R_{wall,meas,exp,ave} - R_{wall,des,exp}\rvert}{R_{wall,des,exp}} \times 100$
		Top	Middle	Bottom	Averaged	
East	6.88	5.93±0.014	6.39±0.016	7.00±0.015	6.44±0.015	6.40
West	6.97	6.71±0.08	7.01±0.09	7.37±0.07	7.03±0.08	0.86

U-values ranged from 4% to 75% in a study by Ref. [44]. [27] reported that the difference could reach up to 20.4% if the results of the theoretical calculations with the measured data using the average method are compared. In addition to the uncertainty in the thermo-physical properties of the walls, the assumption used in the calculations for the design U-value, i.e., disregarding the thermal resistance of the air layer and all other layers between the air layer and external environment (section 2.1), could be another source of error. The thermal resistance of the ventilated cavity and its contribution to the total thermal resistance of the wall structure is further analyzed in the next section.

- Thermal resistance of the ventilated cavity

As it was described in section 2.2, the thermal resistance of the ventilated cavity could be measured following Method 2 by using the cavity surface temperatures and the heat flux through the interior surface of the wall (equation (8)). The plots of the temperature of the interior surface of the cladding $T_{cl,int}$, exterior surface of insulation $T_{ins,ext}$, and their absolute difference measured on different positions of the East and West-oriented cavities of the test facility is shown in Fig. 13. The plots of the heat flux through the interior surface of the walls q_{in} are presented in Fig. 11.

Based on the results, the difference between the cavity surfaces is most of the time lower than 1 °C and does not exceed 2 °C. The temperature values change dynamically depending on the time of the day and the intensity of the solar radiation. Moreover, the difference between the cavity surface temperatures is not similar in all positions along with the height of the walls. The reason is the dynamic variation of the air change rate in the air-space, which consequently causes variation in the temperature distribution inside the air gap. Comparing the East and West-oriented cavities, the plots in Fig. 13 reveal that the temperature profiles are different despite a similar cavity structure. This observation highlights the importance of the microclimate outdoor condition adjacent to the façade, which affects the thermal and hydrodynamic performances of the ventilated cavities behind external claddings with different orientations. The difference in the thermal mass of the materials used in the East and West-oriented walls is another reason for having a different temperature distribution in the air-spaces [12].

The plots of the apparent thermal resistance of the ventilated cavities behind the East and West-oriented external claddings of the test facility are shown in Fig. 14. The results are shown for three positions along with the height of the walls and the corresponding average values. The uncertainty band of the averaged values is also indicated in the plots. According to the results, the apparent thermal resistance of the air gap $R_{cav,app}$ determined in all positions converges to a steady-state value following the definition provided per Method 2. This result is important in the sense of the possibility of achieving a single value of the thermal resistance of the ventilated air-space, which could be used for the code-compliant analysis and eventually implemented in the corresponding standards. The practitioners, therefore, would be able to measure the $R_{cav,app}$ in real applications following a similar procedure described in this study. Based on the results shown in Fig. 14, the converged $R_{cav,app,ave}$ for the East wall and West wall are respectively equal to 0.095 (m^2•K/W) and 0.125 (m^2•K/W), which is 32% higher for the latter. Therefore, the values of $R_{cav,app}$ of the ventilated cavities having a similar geometry are not equal for the walls with different orientations and different thermal inertia. The plots in Fig. 14 reveal that the $R_{cav,app}$ is not similar in all positions along with the height of the walls, which is

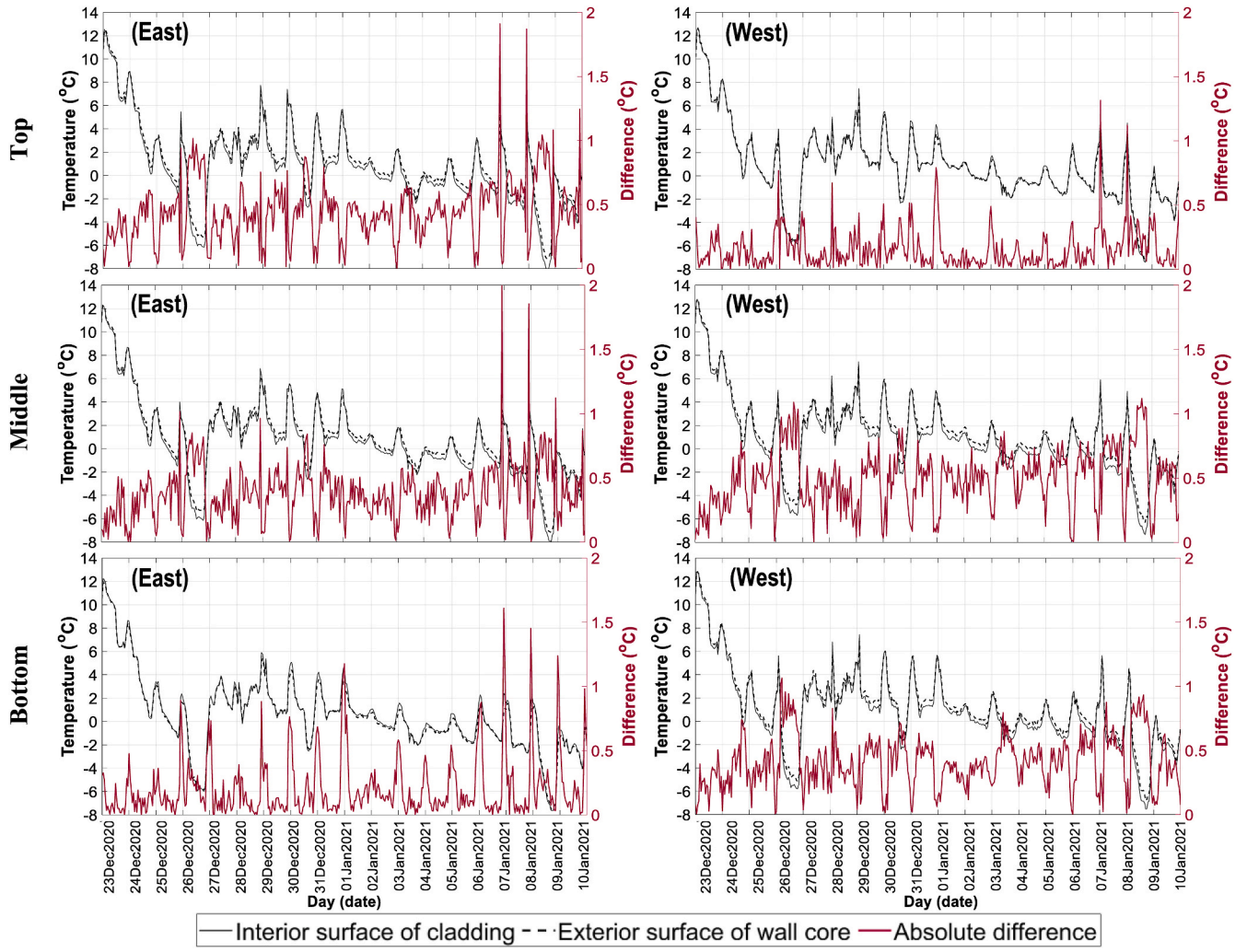

Fig. 13. Cavity surface temperatures (°C) and their absolute difference (°C) measured for the East and West walls of the test facility.

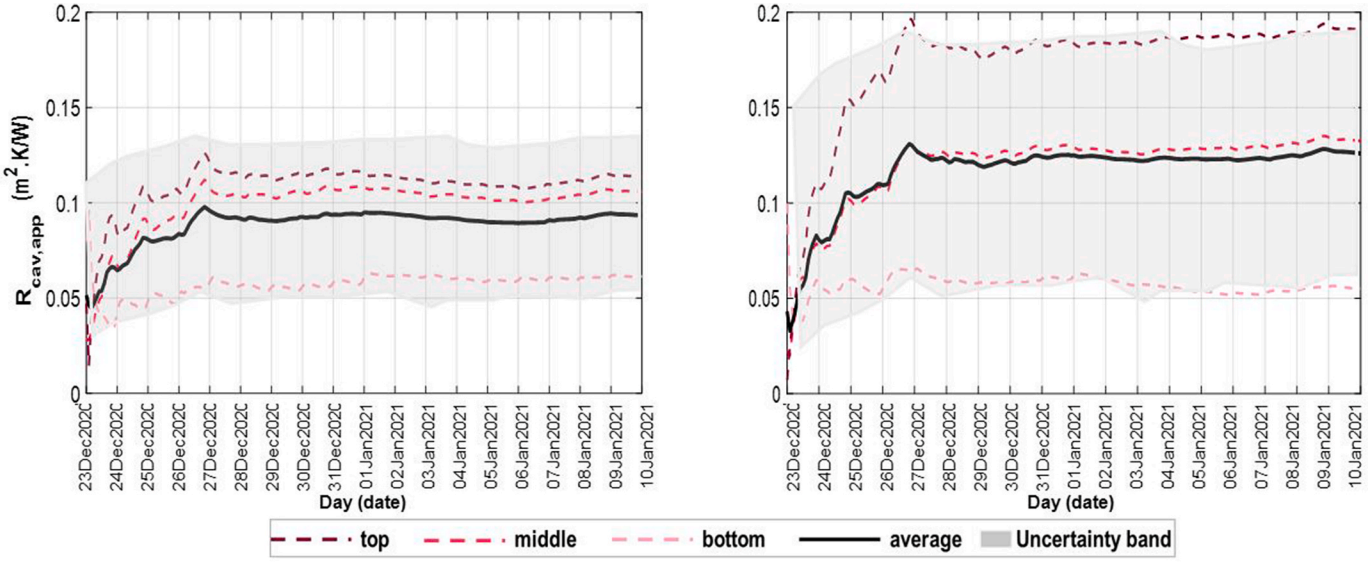

Fig. 14. Thermal resistance of the ventilated cavities measured for the East and West walls of the test facility.

attributed to the difference in the cavity surface temperature and heat flux through the interior surface of the walls, as explained in the previous sections. This observation highlights the need for defining specific measuring points in the wall structure to determine the thermal resistance of the ventilated cavity with an adequate accuracy. It is recommended to install the temperature sensors in the middle of the cavity surfaces along with the height and width of the wall since the airflow regime at this position has become fully developed, and the variation in the thermo-hydro dynamic properties of the air is lower compared to the areas closer to the openings or sides of the wall. Moreover, the plots show that the uncertainty of measurement could reach up to 0.08 (m^2•K/W), which is relatively high compared to the converged values of

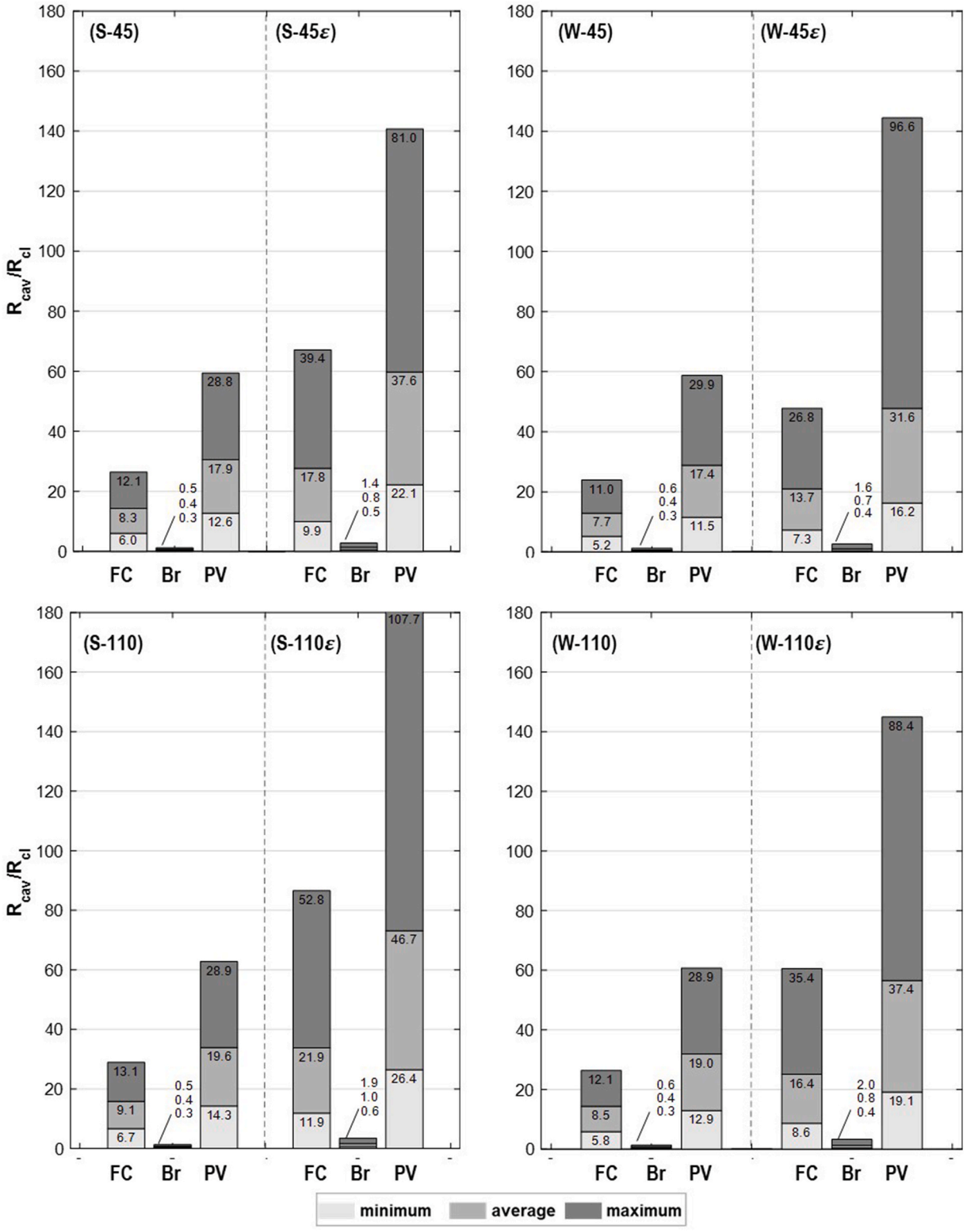

Fig. 15. The ratio of the cavity thermal resistance simulated (minimum, average, and maximum of daily values) over the R-value of claddings (refer to Table 1 for abbreviations).

$R_{cav,app}$. Therefore, it is necessary to use the temperature and heat flux sensors with high accuracy, i.e., with an accuracy equal to or better than ±0.2 °C for temperature and 6% of measurements for heat flux, to reduce the uncertainty of measuring the thermal resistance of the ventilated cavity.

4. Discussion

4.1. Numerical simulations

The ratio of the R_{cav} over the thermal resistance of cladding R_{cl} is plotted using the stack bars presented in Fig. 15. The results are shown considering the minimum, average, and maximum values of R_{cav} during the day of interest to quantify the proportion of the dynamic change of the thermal resistance of the air-space to the R_{cl} of the passive and active façades under different conditions. According to the plots, the ratios are much higher in the BIPV façade compared to the passive claddings with Fiber cement and Brick walls, which is due to the lower R_{cl} of the PV panel. Considering the maximum values in Fig. 15, the results reveal that in the case of using reflective insulation in the cavity with a 110 mm thickness in summer, the ventilated air gap could resist the heat flow through the structure up to 107 times of the active façade. The corresponding values are almost equal to 52 and 2 times, respectively, for the fiber cement and brick claddings; where the higher R_{cl} of the latter compared to the former is the main reason for this difference. Considering the average ratios in the plots, it can be seen that the values in the case of the presence of reflective insulation are almost doubled compared to the cases without having reflective insulation on the cavity surface. The minimum ratios in the plots are also noticeable; the minimum ratio of R_{cav} over R_{cl} could respectively reach up to 6.7, 0.6, and 26.4 times of the fiber cement, brick, and PV claddings. The results presented in Fig. 15 also indicate that the values are generally higher in summer compared to winter, which implies the importance of ventilation in the cavity behind the external claddings in the warm conditions to remove the excess heat from the air-space and prevent the heat flow entering the indoor space. All of the aforementioned observations highlight the significant influence of the ventilated air-space on the thermal resistance of the entire wall structure, which could not have been achieved if the wall assembly had been non-ventilated. In particular, in the case of the active BIPV façades, the presence of the ventilated cavity could have additional benefits in increasing the electrical efficiency of the modules by decreasing the temperature of the PV panels [12], which further underlines the importance of the ventilation behind the active façades.

The contribution of the thermal resistance ventilated air gap to the thermal resistance of the elements used in the wall structure is further analyzed in Table 4. The results are provided considering the ratio of the daily average R_{cav} over the design R-value of fiber plaster $R_{fp,des,sim}$, timber wood $R_{wood,des,sim}$, insulation $R_{ins,des,sim}$, wall core $R_{wc,des,sim}$, wall assembly excluding the surface resistances $R_{wall,des,sim}$, and the total design R-value of the wall structure $R_{tot,des,sim}$. All of the aforementioned design values are calculated based on the procedure described in section 2.1, and the results are provided in Table 1 and section 3.1.

According to Table 4, although most of the ratios do not exceed 0.05, the results in summer conditions with a 110 mm air gap having a layer of reflective insulation reveal that the ventilated air gap could resist the heat flow up to 5 times higher than a 10 mm layer of fiber plaster and up to 0.43 considering a 100 mm layer of timber wood in the core wall. This, alternatively, means that allowing the airflow movement behind the external claddings by using a ventilated cavity could yield a higher impact on the thermal resistance of the wall structure compared to some of the solid layers used in the wall core. It should be noted that the size of the "ventilated air-space" considered in this paper is limited to 150 mm, and wider air gaps typical for Double Skin Facades are not considered, which could have different results in terms of the contribution of the thermal resistance of the cavity to the total thermal resistance of the wall structure.

4.2. Experimental measurements

In this section, the contribution of the measured thermal resistance of the ventilated air-space to the R-value of the elements used in the wall assemblies of the test facility is evaluated. Accordingly, the average value of the measured thermal resistance of the ventilated air-space $R_{cav,app,ave}$ provided in section 3.2 is compared with the design R-value of cladding $R_{cl,des,exp}$, wall core $R_{wc,des,exp}$, wall assembly $R_{wall,des,exp}$ (section 2.4), design total R-value of the wall $R_{tot,des,exp}$, averaged R-value of the wall assembly $R_{wall,meas,exp,ave}$ measured, and averaged total R-value of the wall $R_{wall,meas,exp,ave}$ measured (section 3.2). The ratios are provided in Table 5 for the air-spaces behind the East and West-oriented walls of the test facility.

Based on the results, the thermal resistance of the ventilated air gap is equal to 0.4 and more than 0.6 of the R-value of the external cladding in the East and West-oriented walls, respectively. According to the results presented in section 3.2, the summation of the thermal resistances caused by the air-space and cladding becomes equal to 0.34 (m^2•K/W) and 0.37 (m^2•K/W), respectively, for the East and West walls.

Table 4
The ratio of the daily average cavity thermal resistance simulated over the design R-values of the wall structure with different claddings (refer to Table 1 for abbreviations).

Ratio	Cladding	Condition							
		(S-45)	(S-45ε)	(W-45)	(W-45ε)	(S-110)	(S-110ε)	(W-110)	(W-110ε)
$\frac{R_{cav,ave}}{R_{fp,des,sim}}$	FC	1.91	4.09	1.77	3.14	2.09	5.04	1.95	3.78
	Br	1.83	3.81	1.77	3.24	2.02	4.70	1.94	3.86
	PV	1.86	3.90	1.80	3.27	2.03	4.84	1.97	3.88
$\frac{R_{cav,ave}}{R_{wood,des,sim}}$	FC	0.16	0.35	0.15	0.27	0.18	0.43	0.17	0.32
	Br	0.15	0.32	0.15	0.27	0.17	0.40	0.16	0.33
	PV	0.16	0.33	0.15	0.28	0.17	0.41	0.17	0.33
$\frac{R_{cav,ave}}{R_{ins,des,sim}}$	FC	0.02	0.05	0.02	0.04	0.02	0.06	0.02	0.04
	Br	0.02	0.04	0.02	0.04	0.02	0.05	0.02	0.04
	PV	0.02	0.04	0.02	0.04	0.02	0.05	0.02	0.04
$\frac{R_{cav,ave}}{R_{wc,des,sim}}$	FC	0.02	0.04	0.02	0.03	0.02	0.05	0.02	0.04
	Br	0.02	0.04	0.02	0.03	0.02	0.05	0.02	0.04
$\&\frac{R_{cav,ave}}{R_{wall,des,sim}}$									
	PV	0.02	0.04	0.02	0.03	0.02	0.05	0.02	0.04
$\&\frac{R_{cav,ave}}{R_{tot,des,sim}}$									

Table 5
The ratio of the average cavity thermal resistance measured over R-values of the East and West walls of the test facility.

Wall	$\frac{R_{cav,app,ave}}{R_{jc,des,exp}}$	$\frac{R_{cav,app,ave}}{R_{eb,des,exp}}$	$\frac{R_{cav,app,ave}}{R_{wood,des,exp}}$	$\frac{R_{cav,app,ave}}{R_{ins,des,exp}}$	$\frac{R_{cav,app,ave}}{R_{cl,des,exp}}$	$\frac{R_{cav,app,ave}}{R_{wall,des,exp}}$	$\frac{R_{cav,app,ave}}{R_{tot,des,exp}}$	$\frac{R_{cav,app,ave}}{R_{wall,meas,exp,ave}}$	$\frac{R_{cav,app,ave}}{R_{tot,meas,exp,ave}}$
East	–	–	0.09	0.02	0.40	0.01	0.01	0.01	0.01
West	6.25	2.08	0.12	0.02	0.60	0.02	0.02	0.02	0.02

Considering the corresponding value assumed for the design calculation of the R-value of the ventilated wall structure (section 3.2), i.e., equal to 0.13 ($W/m^2 \bullet K$), it can be seen that the measured values are respectively 1.62 and 1.85 times greater. Although the results in Table 5 indicate that the ratio of $R_{cav,app,ave}$ over most of the thermal resistances in the wall structure does not exceed 0.02, it can be seen that the $R_{cav,app,ave}$ is 2.08 and 6.25 times greater than the R-value of the earth brick and jute coating, respectively, which are used in the West wall to increase its thermal inertia. This observation is noticeable since it implies the important role of the ventilated air-space in providing a layer of thermal insulation for the wall structure despite its lower thermal mass compared to the solid layers. Moreover, the results reveal that the ratio of $R_{cav,app,ave}$ over the common layers used in the East and West walls of the test facility are different, which indicates the impact of the difference in the thermal inertia of the walls and also the difference in the outdoor microclimate conditions adjacent to the façades of a building envelope with different orientations.

It should be pointed out that the impact of the wooden battens in the air-space on the thermal resistance of the cavity is not considered in this study due to its complexity. On one hand, the temperature of the cavity surfaces in the vicinity of the battens could locally increase due to the thermal bridge effect, and on the other hand, the airspeed in the cavity reduces due to the blockage caused by the battens. The effect of the combination of these aspects on the thermal resistance of the cavity needs extra analysis, which could be conducted in future works by installing instruments on different positions of the battens.

5. Conclusion

The dynamic profile of the thermal resistance of the ventilated air-spaces behind passive and active BIPV façades in transient conditions was studied in the present paper. Two definitions were provided to determine the thermal resistance of the cavity using numerical simulations and experimental measurements. The results were compared with the static values calculated based on the [13,23] standards. Despite the limitations of the research, such as using a 2-dimensional geometry with a limited height in the simulations or disregarding the effect of thermal bridges in the measurements, this paper provides certain findings that are important in practice.

In general, the observations in this study highlighted the significant influence of the ventilated air-space on the thermal resistance of the entire wall structure, which could not have been achieved if the wall assembly had been non-ventilated. It was revealed that the thermal resistance of the ventilated air gap is a complex phenomenon that depends on the thermo-hydrodynamic performance of the airflow in the cavity, considering the combined effects of convection and radiation heat transfer. Moreover, it was shown that the behavior of the cavity thermal resistance dynamically changes during a day depending on several parameters, including the outdoor conditions and the thermo-physical properties of the wall. The results indicated that using a thin layer with a low emissivity on the cavity surface adjacent to the wall core could significantly increase the thermal resistance of the air-space. According to the results, the values of the cavity thermal resistance decreased by increasing the airspeed in the cavity. The results of the in-field measurements showed that a converged value for the cavity thermal resistance could be obtained following a similar procedure described in this study. Based on the observations, the temperature and heat flux sensors with a high accuracy shall be used to reduce the uncertainty of measuring the thermal resistance of the cavity. Moreover, it was revealed that the difference in the thermal inertia of the walls and the outdoor microclimate conditions adjacent to the façades of a building with different orientations affect the thermal resistance of the air gap. The results also showed that the contribution of the thermal resistance of the cavity in the wall structure to the overall thermal resistance of the wall could be higher compared to some of the solid layers used in the assembly.

This study was conducted to emphasize that the presence of a ventilated air-space in the wall assembly could have a varying impact on the thermal performance of the structure. As for future studies, the 3-dimensional effects, including the variation of the temperature and airflow through the width of the cavity, could be further evaluated. Moreover, in the case of studying high-rise buildings, the presence of open joints in the external cladding, particularly between the PV modules in the BIPV façades, could affect the thermo-hydrodynamic pattern in the cavity, which requires particular attention in future works. The impact of thermal bridges in the wall assembly on the thermal resistances could also be elaborated on in future studies.

CRediT authorship contribution statement

Mohammad Rahiminejad: Writing – review & editing, Writing – original draft, Visualization, Validation, Software, Methodology, Investigation, Formal analysis, Data curation, Conceptualization. **Dolaana Khovalyg:** Writing – review & editing, Supervision.

Declaration of competing interest

The authors declare that they have no known competing financial interests or personal relationships that could have appeared to influence the work reported in this paper.

Data availability

The data that has been used is confidential.

Acknowledgment

The authors would like to acknowledge the Building Innovation Research and Integration Support group at EPFL (Building 2050) coordinated by Dr. Sergi Aguacil, and the technical unit of the Smart Living Lab in Fribourg (Switzerland) for providing information, drawings, help, and supports on the research test facility CELLS (Controlled Environments for Living Lab Studies) used for the experimental measurements.

References

[1] H.M. Ge, J. Straube, L. Wang, M. Fox, Field study of hygrothermal performance of highly insulated wood-frame walls under simulated air leakage, Build. Environ. 160 (2019), 106202.
[2] C. Agrawal, H. Ge, M. Defo, M. Lacasse, Reliability of Moisture Reference Year (MRY) selection methods for hygrothermal performance analysis of wood-frame walls under historical and future climates, Build. Environ. 207 (2022), 108513.
[3] T. Colinart, M. Bendouma, P. Glouannec, Building renovation with prefabricated ventilated façade element: a case study, Energy Build. 186 (2019) 221–229.
[4] M. Rahiminejad, D. Khovalyg, Impact of the ventilated cavity on the thermal performance of traditional wall structures, Build. Eng. 127 (2021) 187–195.
[5] F. De Masi, V. Festa, A. Gigante, S. Ruggiero, G. Peter, Experimental analysis of grills configuration for an open joint ventilated facade in summertime, J. Build. Eng. 54 (2022), 104608.

[6] S. Wonorahardjo, I. Sutjahja, Y. Mardiyati, et al., Effect of different building façade systems on thermal comfort and urban heat island phenomenon: an experimental analysis, Build. Environ. 217 (2022), 109063.
[7] G.M. Girma, F. Tariku, Experimental investigation of cavity air gap depth for enhanced thermal performance of ventilated rain-screen walls, Build. Environ. 194 (2021), 107710.
[8] B. Nghana, F. Tariku, G. Bitsumlac, Assessing ventilation cavity design impact on the energy performance of rainscreen wall assemblies: a CFD study, Build. Environ. 196 (2021), 107789.
[9] Z. Lin, Y. Song, Y. Chu, An experimental study of the summer and winter thermal performance of an opaque ventilated facade in cold zone of China, Build. Environ. 218 (2022), 109108.
[10] T.G. Theodosiou, A.G. Tsikaloudaki, K.J. Kontoleon, D.K. Bikas, Thermal bridging analysis on cladding systems for building facades, Energy Build. 109 (2015) 377–384.
[11] R. Schindelholz, M. Rahiminejad, A. Chatterjee, D. Khovalyg, Assessment of thermal and electrical performance of BIPV façades using simplified simulations, J. Phys. Conf. 2042 (1) (2021), 012081.
[12] M. Rahiminejad, A. Louis Marie Pàris, H. Ge, D. Khovalyg, Performance of lightweight and heavyweight building walls with naturally ventilated passive and active facades, Energy Build. 256 (2022), 111751.
[13] Iso 6946, Building Components and Building Elements—Thermal Resistance and Thermal Transmittance-Calculation Method, 2017.
[14] M. Rahiminejad, D. Khovalyg, Review on ventilation rates in the ventilated air-spaces behind common wall assemblies with external cladding, Build. Environ. 190 (2021), 107538.
[15] G. Baldinelli, A methodology for experimental evaluations of low-e barriers thermal properties: field tests and comparison with theoretical models, Build. Environ. 45 (2010) 1016–1024.
[16] H. Saber, Practical correlations for the thermal resistance of vertical enclosed airspaces for building applications, Build. Environ. 59 (2013) 379–396.
[17] S.W. Lee, C.H. Lim, I.B. Salleh, Reflective thermal insulation systems in building: a review on radiant barrier and reflective insulation, Renew. Sustain. Energy Rev. 65 (2016) 643–661.
[18] R. Bruno, P. Bevilacqua, V. Ferraro, N. Arcuri, Reflective thermal insulation in non-ventilated air-gaps: experimental and theoretical evaluations on the global heat transfer coefficien, Energy Build. 236 (2021), 110769.
[19] L.E. Aelenei, Thermal Performance of Naturally Ventilated Walls, Ph.D. Dissertation, Universidade Tecnica de Lisboa, 2006.
[20] EXOVA Test Report, Thermal Performance Study for Foam Sheathing Coalition, 2011. Report No. 10 06-M0211-FSC.
[21] B. Meyer, M. Spinu, T. Weston, H. Kuhlman, Impact of low-E WRB facing an air cavity on the R-value of a wall system, ASHRAE 11 (2019) 63–67.
[22] M. Bendouma, T. Colinart, P. Glouannec, H. Noel, Laboratory study on hygrothermal behavior of three external thermal insulation systems, Build. Environ. 210 (2020), 109742.
[23] Iso 9869, Thermal Insulation — Building Elements —In-Situ Measurement of Thermal Resistance and Thermal Transmittance — Part 1: Heat Flow Meter Method, 2014.
[24] R.F. De Masi, V. Festa, S. Ruggiero, G.P. Vanoli, Environmentally friendly opaque ventilated façade for wall retrofit: one year of in-field analysis in Mediterranean climate, Sol. Energy 228 (2021) 495–515.
[25] M. Rahiminejad, D. Khovalyg, Thermal resistance of ventilated air-spaces behind external claddings; definitions and challenges (ASHRAE 1759-RP), Science and Technology for the Built Environment 27 (6) (2021) 788–805.
[26] M. Rahiminejad, D. Khovalyg, Measuring the effective thermal resistance of ventilated air-spaces behind common wall assemblies: theoretical uncertainty analysis and recommendations for the hot box method modifications (ASHRAE 1759-RP), Science and Technology for the Built Environment 28 (3) (2022) 320–337.
[27] K. Gaspar, M. Casals, M. Gangolells, A comparison of standardized calculation methods for in situ measurements of façades U-value, Energy Build. 130 (2016) 592–599.
[28] K. Gaspar, M. Casals, M. Gangolells, In situ measurement of façades with a low U-value: avoiding deviations, Energy Build. 170 (2018) 61–73.
[29] P. Santos, M. Gonçalves, C. Martins, N. Soares, J.J. Costa, Thermal transmittance of lightweight steel framed walls: experimental versus numerical and analytical approaches, J. Build. Eng. 25 (2019), 100776.
[30] Iso 10456, Building Materials and Products — Hygrothermal Properties — Tabulated Design Values and Procedures for Determining Declared and Design Thermal Values, 2010.
[31] R. Garay, B. Arregi, P. Elguezabal, Experimental thermal performance assessment of a prefabricated external insulation system for building retrofitting, Procedia Environmental Sciences 38 (2017) 155–161.
[32] M. Rahiminejad, D. Khovalyg, In-situ measurements of the U-value of a ventilated wall assembly, J. Phys. Conf. (2021) 2069, 012212.
[33] ISO/IEC Guide 98-3, Uncertainty of Measurement – Part 3: Guide to the Expression of Uncertainty in Measurement (GUM:1995), 2008.
[34] F.P. Incropera, Fundamentals of Heat and Mass Transfer, sixth ed., John Wiley & Sons, 2007.
[35] S. Schwab, J. Rime, G. Jaquerod, L. Rinquet, G. Rey, R. Camponovo, et al., Rénovation énergétique: approche globale pour l'enveloppe du bâtiment: études de densification, HEPIA - Genève, 2018, 978-2-9701005-2-2.
[36] M. Ahmed-Dahmane, A. Malek, T. Zitoun, Design and analysis of a BIPV/T system with two applications controlled by an air handling unit, Energy Convers. Manag. 175 (2018) 49–66.
[37] Integrated Environmental Solutions, Reference data, 13th August, https://www.iesve.com, 2021.
[38] R.A. Agathokleous, S.A. Kalogirou, Part I: thermal analysis of naturally ventilated BIPV system: experimental investigation and convective heat transfer coefficients estimation, Sol. Energy 169 (2018) 673–681.
[39] F. Guignard, D. Mauree, M. Lovallo, M. Kanevski, L. Telesca, Fisher-Shannon complexity analysis of high-frequency urban wind speed time series, Entropy 21 (1) (2019) 1–11.
[40] Wladimir Köppen, Translated by Volken, E.; Brönnimann, S. "Die Wärmezonen der Erde, nach der Dauer der heissen, gemässigten und kalten Zeit und nach der Wirkung der Wärme auf die organische Welt betrachtet" [The thermal zones of the earth according to the duration of hot, moderate and cold periods and to the impact of heat on the organic world)], Meteorol. Z. 20 (3) (1884) 351–360 (published 2011).
[41] G. Finch, The Performance of Rainscreen Walls in Coastal British Columbia, University of Waterloo, 2007.
[42] F. Stazi, F. Tomassoni, A. Vegliò, C.D. Perna, Experimental evaluation of ventilated walls with an external clay cladding, Renew. Energy 36 (12) (2011) 3373–3385.
[43] G. Desogus, S. Mura, R. Ricciu, Comparing different approaches to in situ measurement of building components thermal resistance, Energy Build. 43 (2011) 2613–2620.
[44] F. Asdrubali, F. D'Alessandro, G. Baldinelli, F. Bianchi, Evaluating in situ thermal transmittance of green buildings masonries—a case study, Case Stud. Constr. Mater. 1 (2014) 53–59.
[45] ASHRAE 1759 RP, Impact of Air-Flow on Thermal Performance of Air-Spaces behind Cladding, 2020 (Phase 1 of 2).
[46] ASHRAE, Handbook of Fundamentals, SI ed., American Society of Heating, Refrigerating and Air-Conditioning Engineers, Inc, Atlanta, GA, 2021.
[47] ASTM International, C1363-19 Standard Test Method for Thermal Performance of Building Materials and Envelope Assemblies by Means of a Hot Box Apparatus, ASTM International, West Conshohocken, PA, 2019.
[49] Sia, Standardized Data for Building Energy Modeling (SIA 2024), 2015. Zurich, Switzerland.
[50] A.G. Swisspor, Mur extérieur-Mur hors sol- Façade ventilée isolée. Récupéré sur Swisspor, 13th August, https://www.swisspor.ch/, 2021.